

Eccentric orbits and QPOs in neutron star X-ray binaries

D. Marković and F. K. Lamb[★]

Center for Theoretical Astrophysics and Department of Physics, University of Illinois at Urbana-Champaign, 1110 West Green Street, Urbana, IL 61801, USA; markovic@mail.physics.uiuc.edu, f-lamb@uiuc.edu

Submitted 2000 March 23

ABSTRACT

We investigate the suggestion that the frequencies of the kilohertz and other QPOs in the emission from neutron stars in low-mass X-ray binaries are generated by geodesic motion of gas clumps around the star. First we assume, following previous work, that the dominant frequencies produced by such motions are the azimuthal frequency ν_K , the apsidal precession frequency ν_{AP} , and the first overtone of the nodal precession frequency ν_{NP} . We investigate whether geodesics can be found for which these frequencies agree with the observed frequencies. Correcting calculational errors made when the geodesic precession hypothesis was first proposed, we find that ν_K and ν_{AP} disagree qualitatively with the frequencies of the kilohertz QPOs for infinitesimally or even moderately eccentric geodesics. These frequencies are similar to the frequencies of the kilohertz QPOs only for highly eccentric geodesics, with apastron to periastron ratios ~ 3 –4; for these geodesics, $2\nu_{NP}$ differs qualitatively from the frequencies of the low-frequency QPOs. Next we investigate whether these frequencies would be the dominant frequencies produced by orbiting clumps. We find that they are not and that the dominant frequencies are instead harmonics and sidebands of the radial epicyclic frequency ν_r . Finally, we show that gas dynamical constraints restrict the radii of orbiting clumps to be $\ll 10^{-3}$ of the stellar radius; the fractional modulation that could be produced by clumps is therefore $\ll 10^{-6}$. We conclude that there are significant difficulties in interpreting the kilohertz and low-frequency QPOs as consequences of geodesic motion of gas clumps.

Key words: accretion – relativity – stars: neutron – X-rays: stars

1 INTRODUCTION

Observations of low mass X-ray binaries (LMXBs) using the *Rossi X-ray Timing Explorer (RXTE)* satellite have led to the discovery of prominent, narrow features in power spectra of the accretion-powered X-ray emission of these sources, with frequencies ranging from ~ 5 Hz to ~ 1300 Hz (for a review, see van der Klis 2000). High-frequency quasi-periodic oscillations (QPOs) have been observed with frequencies ranging from ~ 500 Hz to ~ 1300 Hz. These ‘kilohertz QPOs’ often appear as a pair of peaks with frequencies ν_1 and ν_2 ($> \nu_1$) that move together and can shift up and down in frequency by up to a factor of two within a few hundred seconds, probably because of changes in the accretion rate. As they shift, ν_1 and ν_2 follow a narrow track in the ν_1 - ν_2 plane that is fixed for a given source. The kilohertz QPOs have frequencies in the range expected for orbital motion near neutron stars and are very likely a strong-field general-relativistic phenomenon.

In six kilohertz QPO sources, oscillations with frequencies of hundreds of Hertz have been observed during X-ray bursts. These ‘burst oscillations’ are almost certainly caused by rotation of brighter regions of the stellar surface at the spin frequency of the star (Strohmayer et al. 1996, 1998; Bildsten 1998; Miller 1999; Strohmayer 1999). Observations indicate that the principal burst oscillation frequency ν_b is the stellar spin frequency ν_s or its first overtone (see, e.g., Strohmayer & Markwardt 1999; Miller 1999).

In four sources, burst oscillations and two simultaneous kilohertz QPOs have both been detected with high confidence. In 4U 1702–43 (Markwardt, Strohmayer & Swank 1998), 4U 1728–34 (Strohmayer et al. 1996; Méndez & van der Klis 1999), and 4U 1636–53 (Zhang et al. 1996; Wijnands et al. 1997a), the difference $\Delta\nu \equiv \nu_2 - \nu_1$ between the frequencies of the two kilohertz QPOs is equal (to within 4–15%) to ν_b . In KS 1731–26 (Wijnands & van der Klis 1997), $\Delta\nu$ is equal (to within $\lesssim 0.7\%$) to one-half ν_b . Careful analysis has shown that in 4U 1636–53, $\Delta\nu$ is slightly but significantly smaller than the spin frequency inferred from its burst oscillations (Méndez, van der Klis & van Paradijs 1998).

[★] Also Department of Astronomy.

2 D. Marković and F. K. Lamb

In some kilohertz QPO sources, the separation frequency $\Delta\nu$ decreases systematically by 30–100 Hz, depending on the source, as ν_2 increases by a much larger amount (Sco X-1: van der Klis et al. 1997; 4U 1608–52: Méndez et al. 1998; 4U 1735–44: Ford et al. 1998; 4U 1728–34: Méndez & van der Klis 1999; see also Psaltis et al. 1998).

The fact that ν_b is close to one or two times $\Delta\nu$ in four sources as well as other evidence motivated the development of the sonic-point beat-frequency (SPBF) model (Miller, Lamb & Psaltis 1998; Lamb & Miller 2000). In this model the frequency ν_2 of the upper kilohertz QPO is close to but less than the general-relativistic orbital frequency ν_{orb} at the sonic radius, where the flow in the disc changes from nearly circular to rapidly inspiraling, whereas the frequency ν_1 of the lower kilohertz QPO is comparable to but less than the beat frequency $\nu_B \equiv \nu_{\text{orb}} - \nu_s$ of the neutron star's spin frequency with ν_{orb} . The transition to hypersonic radial inflow that occurs at the sonic radius R_s in this model is a strong-field general relativistic effect. In the SPBF model, the low-frequency QPOs seen in the Z and atoll sources are produced by interaction of the stellar magnetic field with the disc flow well outside the sonic point, via the magnetospheric beat-frequency mechanism (Alpar & Shaham 1985; Lamb et al. 1985).

The SPBF model explains naturally the existence of only two principal kilohertz QPOs in a given source, the near commensurability of $\Delta\nu$ and ν_b , and the high frequencies, coherence, and amplitudes of these QPOs. The SPBF model predicts that $\Delta\nu$ is less than but close to ν_s and explains naturally the decrease in $\Delta\nu$ with increasing ν_2 seen in some sources (Lamb & Miller 2000). The inward drift of the accretion flow near R_e causes ν_1 to increase faster than ν_2 as the accretion rate increases. Depending on the source, a differential increase of 7% is sufficient to explain the largest observed decrease in $\Delta\nu$.

A strong prediction of the SPBF model is that the neutron star in 4U 1636–536 is not spinning at the ~ 580 Hz frequency of the principal burst oscillation in this source but instead at ~ 290 Hz. This prediction ran counter to what was widely believed at the time (see, e.g., Stella & Vietri 1999), but was confirmed by detection of a ~ 290 Hz subharmonic with an amplitude equal to 40% of the amplitude of the ~ 580 Hz oscillation (Miller 1999). The SPBF model also predicts that the $\nu_2 - \dot{M}$ relation may flatten in some sources when the region of nearly circular flow reaches the innermost stable circular orbit (ISCO). This signature of the ISCO may have subsequently been observed in 4U 1820–30 (Zhang et al. 1998; Kaaret et al. 1999). In the SPBF model, the kilohertz QPOs are a strong-field general relativistic effect and are therefore sensitive probes of the properties of the spacetime near the neutron star, including whether there is an ISCO and the gravitomagnetic torque produced by the spin of the star. Hence, if the model is shown to be correct, measurements of the kilohertz QPOs can be used not only to determine the properties of neutron stars but also to explore gravitational effects in the strong-field regime.

Following the development of the SPBF model, Stella & Vietri (1998; see also Morsink & Stella 1999) proposed that the 10–60 Hz low-frequency QPOs (LFQPOs) and bumps observed in power spectra of the X-ray emission from the atoll sources and, possibly, the horizontal branch oscillations (HBOs) observed in the Z sources (which are observed

Table 1. Proposed QPO frequency identifications.

QPO Frequency	Geodesic Frequency
ν_{HBO} or ν_L	Nodal precession frequency ν_{NP} or $2\nu_{\text{NP}}$
ν_1	Apsidal precession frequency ν_{AP}
ν_2	Azimuthal frequency ν_K

simultaneously with the kilohertz QPOs; see van der Klis 2000) might be the first or second harmonics of the nodal precession frequency ν_{NP} of gas clumps moving on slightly inclined, *infinitesimally eccentric geodesics* (IEGs) with azimuthal frequencies equal to ν_2 , around neutron stars with the 250–350 Hz spin rates inferred from the burst oscillations and the SPBF model. For such stars, nodal precession is driven by the prograde gravitomagnetic (Lense–Thirring) torque, but is partially offset by the retrograde torque produced by the star's rotation-induced quadrupolar distortion.

Recent work on the global modes of viscous accretion discs (Marković & Lamb 1998) has demonstrated that such discs have a dense spectrum of gravitomagnetically precessing modes that are localised near the inner boundary of the region of nearly circular flow. The highest-frequency of these modes precesses with a frequency only slightly lower than the nodal precession frequency ν_{NP} of a test particle orbiting at the same radius. Contrary to what had been expected since the pioneering work of Bardeen & Petterson (1975), the first few of these modes are very weakly damped and may therefore be excited, producing detectable variations in the X-ray emission (Marković & Lamb 1998; see also Armitage & Natarajan 1999). However, further work (Psaltis et al. 1999a; Morsink & Stella 1999; Kalogera & Psaltis 1999) has shown that the frequencies and frequency behaviors of the LFQPOs and HBOs are inconsistent with the proposal of Stella & Vietri (1998) that these frequencies are the first or second harmonics of the nodal precession frequency of the IEG with azimuthal frequencies $\sim \nu_2$ around stars with the 250–350 Hz spin rates inferred from the burst oscillations and the SPBF model.

Stella & Vietri (1999; hereafter SV) subsequently proposed that ν_2 and ν_1 are the azimuthal and apsidal precession frequencies ν_K and ν_{AP} of gas clumps orbiting the star on eccentric geodesics; $\nu_{\text{AP}} = \nu_K - \nu_r$ in terms of the radial epicyclic frequency ν_r . They again proposed that the frequencies ν_{HBO} and ν_L of the low-frequency QPOs and bumps seen in power spectra of the Z and atoll sources are the first or second harmonics of the nodal precession frequency ν_{NP} of these same geodesics, but argued that ν_s is may be $\gg 300$ Hz to give better agreement of ν_{NP} with ν_{HBO} and ν_L . The frequency identifications proposed by SV are listed in Table 1. SV simply assumed that radiating or obscuring gas clumps with the required properties form near the star; that hydrodynamic, radiation, and magnetic forces are negligible, so that the gas clumps move on geodesics; that $2\nu_{\text{NP}}$, ν_{AP} , and ν_K are the dominant frequencies generated by clumps in purely geodesic motion about a neutron star; and that all the clumps move on geodesics with the same periastron and apastron radii r_p and r_a . The large variations of ν_{HBO} or ν_L , ν_1 , and ν_2 that occur in the indi-

vidual sources are attributed to gas clumps being fed onto different geodesics at different times.

SV first pointed out that the frequencies ν_{AP} and ν_{K} of infinitesimally eccentric geodesics (IEGs) around nonrotating stars with masses of $1.8\text{--}2.2 M_{\odot}$ are comparable to the values of ν_1 and ν_2 observed in Sco X-1, although they do not track the tightly correlated variation of ν_1 and ν_2 (see their Fig. 1). Stella & Vietri then argued that sequences of moderately eccentric geodesics (MEGs) would give apsidal precession and azimuthal frequencies more consistent with the observed frequencies of the kilohertz QPOs.

Once geodesics of finite eccentricity are allowed, the geodesic precession hypothesis does not by itself predict a relation between ν_{AP} and ν_{K} . The reason is that the characteristic frequencies of such geodesics are functions of two parameters: r_{p} and r_{a} . The set of geodesics that satisfy $r_{\text{a}} \geq r_{\text{p}} > R_{\text{e}}$ generate frequencies that cover a wide area in the two-dimensional $\nu_{\text{AP}}\text{-}\nu_{\text{K}}$ plane, rather than a one-dimensional curve. In order to obtain a $\nu_{\text{AP}}\text{-}\nu_{\text{K}}$ relation that could explain the tightly correlated variation of ν_1 and ν_2 , some physical constraint is needed that will convert the two-parameter set of allowed geodesics to a one-parameter allowed sequence of geodesics that generates a curve in the $\nu_{\text{AP}}\text{-}\nu_{\text{K}}$ plane relating ν_{AP} and ν_{K} .

SV addressed this issue by proposing that some physical mechanism keeps r_{p} constant in a given source while r_{a} varies. They suggested that r_{p} may remain constant because it is equal to the radius r_{isco} of the innermost stable circular orbit, to the radius r_m at which the magnetic field of the star first couples to the accreting gas, or to the equatorial radius R_{e} of the neutron star. However, the periastron radius of an eccentric geodesic can be significantly smaller than r_{isco} (see Marković 2000) and the magnetic coupling radius r_m varies as the accretion rate varies (see Lamb 1989).

SV reported that they were able to construct MEG sequences with apsidal precession and azimuthal frequencies that agree approximately with the kilohertz QPO frequencies observed in Sco X-1, assuming that r_{p} is constant but can have any value greater than r_{isco} . However, as we explain in Section 3.1 and the Appendix, SV computed ν_{K} incorrectly. Karas (1999) noticed this error (see his footnote 2), but thought that its effect was small because the geodesics that SV considered have small eccentricities $\epsilon \sim 0.1$, which corresponds to $r_{\text{a}}/r_{\text{p}} = 1.2$. However, in order to fit the data, ν_{r} must be $\lesssim 0.3 \nu_2$. A given clump therefore makes only a small fraction of its full radial excursion during each orbit of the star and hence—in contrast to the behavior of particles in similar Newtonian orbits—the variation with radius of its rate of azimuthal phase advance does not average out. The error made in SV therefore produced a 10% (≈ 100 Hz) error in ν_{K} , which is very large compared to the uncertainties in ν_2 for Sco X-1. When the correct values of ν_{K} are used, the MEG sequences cited by SV give $\nu_{\text{AP}}\text{-}\nu_{\text{K}}$ relations that disagree qualitatively with the Sco X-1 frequency data (see Section 3.1). SV did not consider the frequency data available on other sources.

Motivated by the proposal of SV, Karas (1999) investigated whether geodesic sequences can be constructed which give $\nu_{\text{r}}\text{-}\nu_{\text{K}}$ relations that agree with the $\Delta\nu\text{-}\nu_2$ correlations observed in Sco X-1 and 4U 1608–52, if M is treated as a free parameter for each source and r_{p} and r_{a} are freely chosen for each measurement of ν_1 and ν_2 . Karas also in-

vestigated whether geodesic sequences can be constructed which give $\nu_{\text{r}}\text{-}\nu_{\text{AP}}$ relations that agree with the $\Delta\nu\text{-}\nu_2$ correlations observed. This assumes that the principal kilohertz QPO frequencies are $\nu_{\text{K}} - 2\nu_{\text{r}}$ and $\nu_{\text{K}} - \nu_{\text{r}}$; its physical motivation is unclear. Karas considered only nonrotating masses (he did not construct any stellar models) and allowed highly eccentric geodesics (ϵ up to 0.4, which corresponds to $r_{\text{a}}/r_{\text{p}} = 2.3$). Not surprisingly, given that varying r_{p} and r_{a} allows coverage of a large area of the $\nu_{\text{r}}\text{-}\nu_{\text{K}}$ plane (see above), he found that fits are possible, although he did not report the parameters or the value of χ^2/dof for any individual fits. Such fits imply that r_{a} is always a function of r_{p} , i.e., that specifying r_{p} uniquely specifies a particular eccentric geodesic. Moreover, the function $r_{\text{a}} = r_{\text{a}}(r_{\text{p}})$ must be different for every source. The physical motivation for this is unclear. For some fits, Karas assumed that a clump only needs to complete 92%–97% of the radial extent of its geodesic, because of the clump’s finite size. The physical basis of this assumption is unclear.

Psaltis, Belloni & van der Klis (1999b) have pointed to a possible correspondence between features in the power spectra of black holes and neutron stars in LMXBs, emphasising the similar properties of the 0.1–100 Hz QPOs observed in the atoll sources, Cir X-1, and some black hole sources and the 15–60 Hz HBOs seen in the Z sources. Somewhat more speculatively, Psaltis et al. suggested that the power spectral ‘humps’ sometimes observed at 10–60 Hz in black hole sources may be related to the lower-frequency members of the two kilohertz QPOs seen in the Z and atoll sources, which have frequencies $\nu_1 \sim 300\text{--}800$ Hz.

Motivated by the results of Psaltis et al. (1999b), Stella, Vietri & Morsink (1999; hereafter SVM) compared the frequencies of IEGs around neutron stars and black holes with the frequencies of QPOs and other features observed in neutron star and black hole LMXBs. Assuming that ν_{K} , ν_{AP} , and $2\nu_{\text{NP}}$ are the dominant frequencies produced by gas clumps moving on such IEGs, that the spin rates of the neutron stars in LMXBs range from 300 to 900 Hz, and that the dimensionless angular momenta $j \equiv cJ/GM^2$ of the black holes in LMXBs range from 0.1 to 0.3 (here J and M are the angular momentum and mass of the black hole), SVM showed that there are IEGs around $1.95 M_{\odot}$ neutron stars which give values of ν_{K} , ν_{AP} , and $2\nu_{\text{NP}}$ that agree within factors ~ 2 with the frequencies of the kilohertz and lower-frequency QPOs observed in neutron star LMXBs and that there are IEGs around black holes which give values of $2\nu_{\text{NP}}$ and ν_{AP} that agree within factors ~ 2 with the frequencies of the 0.1–10 Hz and 2–300 Hz features observed in the power spectra of some black hole LMXBs. However, SVM did not attempt to fit any frequency data.

Recently, Psaltis & Norman (2000) proposed a model of QPOs in neutron star and black hole LMXBs based on the assumption that there is a ‘resonant ring’ in the inner accretion disc. A ring with the properties proposed has a dense spectrum of resonances, including resonances at the frequencies $2\nu_{\text{NP}}$, ν_{AP} , and ν_{K} of an IEG at the radius of the ring. Psaltis & Norman assumed that these three frequencies are the dominant frequencies produced by the resonant ring and identified them with the frequencies of the low-frequency and kilohertz QPOs in the neutron star LMXBs.

If it could be established that the frequencies of the most prominent QPOs and other features observed in power

Table 2. Types of the geodesics considered in the present work.

Quantity	Infinitesimally Eccentric Geodesics (IEGs)	Geodesics with Finite Eccentricities ^a
Periastron radius r_p	Equal to r_a	Fixed for a given source; varies from source to source
Apastron radius r_a	Freely chosen for each frequency pair	Freely chosen for each frequency pair

^aWe refer to geodesics with finite eccentricities as moderately eccentric geodesics (MEGs) if $r_a < 1.5 r_p$ ($\epsilon < 0.2$) or as highly eccentric geodesics (HEGs) if $r_a > 1.5 r_p$ ($\epsilon > 0.2$).

spectra of the X-ray emission from neutron star and black hole LMXBs are simply the characteristic frequencies of test particle geodesics around these objects, measurements of these frequencies would provide a very simple way to explore the effects of strong-field gravity. Moreover, as discussed by Marković (2000), the periastron radius of an eccentric geodesic can be smaller than the radius of the ISCO. Hence, if the highest frequency QPOs could be shown to be produced by clumps of gas moving on geodesics with substantial eccentricities, it might be possible to derive even tighter upper bounds on the radii of the neutron stars in the kilohertz QPO sources and hence on the hardness of the equation of state of neutron star matter than have been derived from the models in which the frequencies of the upper kilohertz QPOs are the orbital frequencies of gas in nearly circular orbits (Miller et al. 1998; Schaab & Weigel 1999). On the other hand, by rejecting any causal connection between the frequency difference $\Delta\nu$ and the stellar spin frequency ν_s , such a model would leave unexplained the origin of the burst oscillations and the closeness of $\Delta\nu$ to the burst oscillation frequency.

In the present paper we investigate further the possibility that the frequencies of various QPOs and other features in power spectra of the X-ray emission from neutron stars in LMXBs are certain frequencies of special geodesics around these stars. For the purposes of this analysis, we simply assume that gas clumps with the required properties can be formed and destroyed in the required way; that they are injected onto the required geodesics; and that once injected, the motion of the clumps is unaffected by radiation, magnetic, or gas pressure forces, so that their motion is purely geodesic. We then explore whether geodesic frequencies are consistent with the observed QPO frequencies; compute the oscillation frequencies that would be produced by emitting, reflecting, or obscuring clumps moving on geodesics around a neutron star; and analyze the constraints imposed on such models by basic gas dynamics. We consider the geodesics and frequency identifications proposed by SV, SVM, Karas (1999), and Psaltis & Norman (2000), but we do not restrict ourselves to these models. The various types of geodesics we study are listed in Table 2.

In Section 2 we describe how we compute the neutron star models, spacetimes, and geodesics that we need and the procedure we use to construct the geodesic frequency relations that fit best the measured QPO frequencies.

In Section 3 we investigate whether certain geodesic frequencies are consistent with the frequencies of the power spectral features observed in the atoll and Z sources. For the purposes of this analysis, we simply assume that clumps moving on geodesics produce X-ray oscillations with the frequencies ν_K , ν_{AP} , and $2\nu_{NP}$, and then examine whether one

can construct geodesics for which these frequencies agree with the observed frequencies. We find that the ν_{AP} - ν_K relations given by the best-fitting sequences of IEGs and MEGs are qualitatively different from the observed ν_1 - ν_2 correlations, for any acceptable neutron star models and spin rates. We therefore explore whether dropping the requirement that geodesics be only moderately eccentric would allow acceptable fits. We show that ν_{AP} - ν_K relations similar to the observed kilohertz QPO frequency correlations are possible using highly eccentric geodesics (HEGs), but only if the geodesic sequences include HEGs with apastron to periastron ratios $\gtrsim 3$; most of the best-fitting frequency relations are, however, formally unacceptable. We find that frequencies other than ν_{AP} and ν_K produce frequency relations that disagree qualitatively with observed kilohertz QPO frequency correlations.

Next, we examine whether sequences of HEGs can be found that give $2\nu_{NP}$ - ν_K and ν_{AP} - ν_K relations that are simultaneously consistent with the frequencies of the low-frequency QPOs and the kilohertz QPOs. We find that the best-fitting $2\nu_{NP}$ - ν_K and ν_{AP} - ν_K relations disagree qualitatively with the observed correlations, for realistic neutron star models and physically allowed spin frequencies.

We also investigate whether there are sequences of geodesics that give $2\nu_{NP}$ - ν_{AP} relations consistent with the frequencies of the low- and high-frequency spectral features observed in Cir X-1. Geodesics can be found that give relations consistent with most of the Cir X-1 frequency data, but only geodesics around neutron stars with very low masses ($M \sim 1.3 M_\odot$) and high spin rates (900 Hz) have frequencies that also approach the frequencies of the highest-frequency QPOs observed in Cir X-1.

In Section 4 we compute numerically the X-ray oscillation frequencies that would be generated by occulting, reflecting, and radiating clumps moving on geodesics around a neutron star by simulating the waveforms produced by such clumps. We find that contrary to what has been assumed in previous work, most of the power generated by orbiting clumps appears in peaks of roughly equal total power at the radial epicyclic frequency ν_r , at $\nu_K + \nu_r$, and at $\nu_K + 2\nu_r$. There is power at ν_K , but it is always $\lesssim 25\%$ of the power in each of the three dominant peaks and there are often many other peaks as strong or stronger than the peak at ν_K . For the relevant geodesics, the power at ν_{AP} and at ν_{NP} generated by most mechanisms is $\lesssim 10\%$ of the power in the dominant peaks. We were unable to find any effect or geometry that produces significant power at $2\nu_{NP}$.

In Section 5 we explore the constraints on orbiting clump models and on the amplitude of the X-ray modulation that can be generated in such models imposed by basic gas dynamics. We find that gas dynamical constraints require

the size of an individual clump to be a fraction $\lesssim 10^{-3}$ of the stellar radius and the density of the gas in the clumps to be $\gg 10^5$ times the interclump density and $\gg 10^6$ times the mean density near the star. As a result, the maximum X-ray modulation that clumps could produce is $\ll 10^{-6}$.

In Section 6 we discuss our principal results and conclude that there are significant difficulties with the geodesic precession and resonant ring models of the kilohertz and other QPOs.

2 COMPUTATION OF GEODESICS AND FREQUENCY COMPARISON PROCEDURE

2.1 Computation of geodesics

We first computed numerically a large suite of neutron star models and spacetimes for a range of neutron-star matter equations of state (EOS), stellar spin rates, and masses. We then integrated the equations of bound geodesic motion (see Marković 2000) in the exterior spacetimes of these neutron star models to determine the characteristic frequencies and other properties of possibly relevant geodesics.

Modern numerical codes (Komatsu, Eriguchi & Hachisu 1989a, 1989b; Cook, Shapiro & Teukolsky 1992, 1994a, 1994b; Stergioulas & Friedman 1995; Nozawa et al. 1998) allow accurate construction of uniformly spinning, equilibrium stellar models using any tabulated EOS. We use the particular variant developed by Stergioulas & Friedman (1995). With the exception of Cir X-1, the neutron star models that give the best fits to the frequency correlations we consider in this paper all have masses $> 1.7 M_\odot$ and spin rates < 600 Hz, substantially lower than their mass-shedding limits.

We considered a range of neutron star matter equations of state. We find that stars constructed using the modern, realistic EOS A18+UIX+ δv_b (Akmal, Pandharipande & Ravenhall 1998; Pandharipande, Akmal & Ravenhall 1998) give geodesics that are almost identical to those given by the earlier realistic UU EOS of Wiringa, Fiks & Fabrocini (1988). In order to facilitate comparison with previous work, we mostly report results based on the UU EOS. In order to explore the effects of uncertainties in the EOS, we also studied stars constructed using the early EOS of Bethe & Johnson (1974; EOS C in the compilation by Arnett & Bowers 1977), which is softer than the UU EOS at high densities. In order to allow comparison with previous work that used this EOS (e.g., SV), we also investigated stars based on an early mean-field EOS constructed by Pandharipande & Smith (1975; EOS L in Arnett & Bowers 1977), even though this EOS is now considered unrealistically hard. These three equations of state are discussed in more detail in the companion paper (Marković 2000).

2.2 Construction of frequency relations

The frequencies ν_{NP} , ν_{AP} , and ν_{K} of a geodesic are functions of its periastron and apastron radii r_p and r_a (we use circumferential radii everywhere), the EOS of neutron star matter, and the mass M and dimensionless angular momentum $j \equiv cJ/GM^2$ of the neutron star. For a given EOS and M , j is a function of the neutron star spin rate ν_s , which

may be directly observable. We therefore parameterise the effects of stellar rotation by ν_s .

For infinitesimally eccentric geodesics, we assume that the sequence $\{r_{a,i}\}$ of apastron radii is the same as the sequence $\{r_{p,i}\}$ of periastron radii and then use the maximum likelihood method to determine the $\{r_{p,i}\}$ sequence that gives the $\nu_{\text{AP}}-\nu_{\text{K}}$ sequence that best fits the observed $\nu_1-\nu_2$ sequence. We treat each $r_{p,i}$ as a free parameter, requiring only that it exceed r_{isco} .

For geodesics with finite eccentricities, the i th members of the sequences $\{\nu_{\text{NP},i}\}$, $\{\nu_{\text{AP},i}\}$, and $\{\nu_{\text{K},i}\}$ depend on both $r_{p,i}$ and $r_{a,i}$. Hence the geodesic precession hypothesis does not by itself predict a relation between the different characteristic frequencies of a geodesic. As explained in the Introduction, some physical constraint is needed that will convert the two-parameter set of geodesics specified by r_p and r_a to a single-parameter sequence of geodesics that will generate a curve in, e.g., the $\nu_{\text{AP}}-\nu_{\text{K}}$ plane. We follow Stella & Vietri (1999) in assuming that r_p is constant in a given source but that it can be chosen freely for each source to give the best possible fit of the $k\nu_{\text{NP}}-\nu_{\text{K}}$ and $\nu_{\text{AP}}-\nu_{\text{K}}$ relations to the observed frequency correlations (we require only that r_p exceed the equatorial radius R_e of the star, if there is no marginally bound geodesic, or that r_p exceed r_{mb} , the periastron radius of the marginally bound geodesic). Here k ($= 1$ or 2) is the harmonic of the nodal precession frequency that the hypothesis identifies with ν_{HBO} or ν_{L} . For a given r_p , the frequencies ν_{NP} , ν_{AP} , and ν_{K} are continuous functions of r_a . We assume that the r_a sequence for each source can be chosen freely to give the best possible agreement of the $k\nu_{\text{NP}}$, ν_{AP} , and ν_{K} sequences with, e.g., the observed ν_{HBO} , ν_1 , and ν_2 sequences. We determine which r_a sequence agrees best with the frequency data using the maximum likelihood method. We refer to geodesics with finite eccentricities as moderately eccentric if $r_{a,\text{max}}/r_p < 1.5$ and as highly eccentric if $r_{a,\text{max}}/r_p > 1.5$ (see Table 2).

For each EOS, we treat M as a free parameter within the mass range allowed by the EOS. The variation of ν_{AP} with ν_{K} is relatively insensitive to the spin rate of the star, unless the stellar mass required is near the maximum stable mass, in which case nonzero spin makes the fits significantly worse. In contrast, the variation of ν_{NP} with ν_{K} is sensitive to the spin of the star. In order to give the geodesic precession hypothesis the best possible chance of fitting the data, we treat ν_s as a free parameter, allowing any value between zero and the mass-shedding limit, even though the neutron stars in the kilohertz QPO sources are thought to have spin frequencies ~ 250 –350 Hz.

We assume that a necessary (although clearly not sufficient) condition for the geodesic precession hypothesis to be acceptable is that the best-fitting sequence of geodesics gives frequencies consistent with the QPO frequencies observed in all the sources to which the hypothesis is supposed to apply. In assessing whether the frequencies given by a particular geodesic sequence are consistent with the observed frequencies of the relevant QPOs, we use the frequency uncertainties reported in the literature. These uncertainties generally include only statistical errors. We caution that when a QPO or other feature is weak, systematic errors introduced, for example, by uncertainties in the continuum, are likely to be significant.

2.3 Fits to kilohertz QPOs

Consider first the kilohertz QPOs. Suppose there are n simultaneous measurements of the two kilohertz QPO frequencies ν_1 and ν_2 and let $\nu_{1,i}$ and $\nu_{2,i}$ denote, respectively, the i th (simultaneous) pair of measurements. We assume that the errors in $\nu_{1,i}$ and $\nu_{2,i}$ are normally distributed with standard deviations $\sigma_{1,i}$ and $\sigma_{2,i}$. Then the likelihood of any given set of the parameters M , ν_s , $\{r_{p,i}\}$, and $\{r_{a,i}\}$ is

$$\mathcal{L}(M, \nu_s, \{r_{p,i}\}, \{r_{a,i}\}) \equiv - \prod_{i=1}^n \frac{1}{2\pi\sigma_{1,i}\sigma_{2,i}} \times \times \exp \left[-\frac{(\nu_{1,i} - \nu_{\text{AP},i})^2}{2\sigma_{1,i}^2} - \frac{(\nu_{2,i} - \nu_{\text{K},i})^2}{2\sigma_{2,i}^2} \right], \quad (1)$$

where $\{\nu_{\text{AP},i}\}$ and $\{\nu_{\text{K},i}\}$ are the apsidal precession and azimuthal frequency sequences given by the EOS, M , ν_s , and the radius sequences $\{r_{p,i}\}$, and $\{r_{a,i}\}$.

We characterise the goodness of a fit by $\chi^2/\text{dof} \equiv \hat{\chi}^2/m$, where $\hat{\chi}^2$ is twice the sum of the squared terms in the exponential in equation (1) and m is the number of degrees of freedom. For n data points ($2n$ frequencies), fits of infinitesimally eccentric geodesics have $n+2$ parameters (the $\{r_{a,i}\}$ plus M and ν_s), or $n+1$ parameters if the spin is fixed *a priori*, so $m = 2n - n - 2 = n - 2$, or $n - 1$ if the spin is fixed; fits of geodesics with finite eccentricities have $n+3$ parameters (the $\{r_{a,i}\}$ plus r_p , M , and ν_s) or $n+2$ if the spin is fixed, so $m = n - 3$, or $n - 2$ if the spin is fixed.

We begin by picking an EOS and spin frequency ν_s . The frequencies ν_{AP} and ν_{K} depend only on the exterior spacetime close to the rotation equator and are single-valued, continuous functions of r_p and r_a . As shown in the companion paper (Marković 2000), the exterior spacetime close to the rotation equator of a star with mass M and spin frequency ν_s can be described by the eight metric functions $\rho_o(M, \nu_s, s)$, $\alpha_o(M, \nu_s, s)$, $\beta_o(M, \nu_s, s)$, $\gamma_o(M, \nu_s, s)$, $\bar{\rho}(M, \nu_s, s)$, $\bar{\alpha}(M, \nu_s, s)$, $\bar{\beta}(M, \nu_s, s)$ and $\bar{\gamma}(M, \nu_s, s)$, where $s \equiv r/(r+R_e)$. We determine these metric functions for each ν_s and each $M < M_{\text{max}}(\nu_s)$ that we consider, by interpolating in a sequence of metric functions computed previously for this value of ν_s and a sufficiently dense sequence $\{M_i\}$ of stellar masses. Here $M_{\text{max}}(\nu_s)$ is the maximum stable mass for stars of spin frequency ν_s .

Once the metric functions are known, we can compute ν_{AP} and ν_{K} as functions of r_p and r_a . For infinitesimally eccentric geodesics, we determine numerically the sequence $\{r_{a,i}\}$ of r_a values that, with $r_{p,i} = r_{a,i}$, maximises \mathcal{L} . For geodesics with finite eccentricities, we determine the sequence $\{r_{a,i}\}$ that maximises \mathcal{L} for a given r_p . We then vary r_p and M to find the values that give the largest maximum value of \mathcal{L} . As noted above, the $\nu_{\text{AP}}\text{-}\nu_{\text{K}}$ relation given by a particular sequence of geodesics is fairly insensitive to ν_s and hence the quality of the fit to the $\nu_1\text{-}\nu_2$ correlation observed in a given source varies only slightly over a wide range of spin rates. We therefore do not attempt to determine the best-fit spin frequency accurately, but instead quote a range of spin frequencies that have similar likelihoods.

Although we fit the $\nu_{\text{AP}}\text{-}\nu_{\text{K}}$ relations allowed by a given geodesic precession hypothesis to the $\nu_1\text{-}\nu_2$ data as described above, in our figures we compare the relation between $\nu_r = \nu_{\text{K}} - \nu_{\text{AP}}$ and ν_{K} given by the best-fitting se-

quence of geodesics with the observed correlation between $\Delta\nu \equiv \nu_2 - \nu_1$ and ν_2 , because one can assess the goodness of the fits much more easily by examining such plots. The uncertainties in $\Delta\nu$ shown in these plots were not used in the fitting procedure and are shown only to give an approximate visual impression of the goodness of fit; they were computed by adding the uncertainties in ν_1 and ν_2 in quadrature.

2.4 Fits to kilohertz and low-frequency QPOs

Consider now the spectral features at ν_{HBO} or ν_{L} . We wish to determine whether a sequence of geodesics can be constructed that gives $k\nu_{\text{NP}}\text{-}\nu_{\text{K}}$ and $\nu_{\text{AP}}\text{-}\nu_{\text{K}}$ relations that are simultaneously consistent with, e.g., the observed $\nu_{\text{HBO}}\text{-}\nu_2$ and $\nu_1\text{-}\nu_2$ correlations. For a given EOS, the parameters are the same as for the kilohertz QPOs alone, but their likelihood is now

$$\mathcal{L}(M, \nu_s; \{r_{p,i}\}, \{r_{a,i}\}) \equiv - \prod_{i=1}^n \frac{1}{2\pi\sigma_{1,i}\sigma_{2,i}\sigma_{\text{HBO},i}} \times \times \exp \left[-\frac{(\nu_{1,i} - \nu_{\text{AP},i})^2}{2\sigma_{1,i}^2} - \frac{(\nu_{2,i} - \nu_{\text{K},i})^2}{2\sigma_{2,i}^2} - \frac{(\nu_{\text{HBO},i} - k\nu_{\text{NP},i})^2}{2\sigma_{\text{HBO},i}^2} \right], \quad (2)$$

where $\nu_{\text{NP},i} \equiv \nu_{\text{NP}}(M, \nu_s, r_{p,i}, r_{a,i})$. In contrast to ν_{AP} and ν_{K} , ν_{NP} depends sensitively on ν_s and hence we can determine fairly accurately the spin frequency that gives the best fit.

We again characterise the goodness of a fit by $\chi^2/\text{dof} \equiv \hat{\chi}^2/m$, where $\hat{\chi}^2$ is twice the sum of the squared terms in the exponential in equation (2) and m is the number of degrees of freedom. For n data points ($3n$ frequencies), fits of infinitesimally eccentric geodesics have $m = 2n - 2$, or $2n - 1$ if the spin is fixed; fits of geodesics with finite eccentricities have $m = 2n - 3$, or $2n - 2$ if the spin is fixed.

3 FREQUENCY RELATIONS

We now investigate whether sequences of geodesics can be found that have characteristic frequencies which agree with the frequencies of the kilohertz QPOs observed in the Z and atoll sources. We first explore whether it is possible to construct sequences of IEGs or MEGs (see Table 2) that give $\nu_{\text{AP}}\text{-}\nu_{\text{K}}$ relations consistent with the observed correlations of ν_1 with ν_2 . We find that no such sequences exist for acceptable neutron star models and spin rates. We also show that the behavior of other characteristic frequencies, such as ν_{K} and $\nu_r + \nu_{\text{K}}$, is inconsistent with the observed $\nu_1\text{-}\nu_2$ correlations for geodesics of any eccentricity. We therefore consider whether allowing highly eccentric geodesics (HEGs) would make it possible to construct geodesic sequences that give $\nu_{\text{AP}}\text{-}\nu_{\text{K}}$ relations consistent with the observed $\nu_1\text{-}\nu_2$ correlations. We also explore whether there are sequences of HEGs with $\nu_{\text{AP}}\text{-}\nu_{\text{K}}$ and $2\nu_{\text{NP}}\text{-}\nu_{\text{K}}$ relations that are simultaneously consistent with the observed $\nu_1\text{-}\nu_2$ and $\nu_{\text{L}}\text{-}\nu_{\text{K}}$ or $\nu_{\text{HBO}}\text{-}\nu_{\text{K}}$ correlations. Finally, we investigate the frequency correlations observed in Cir X-1.

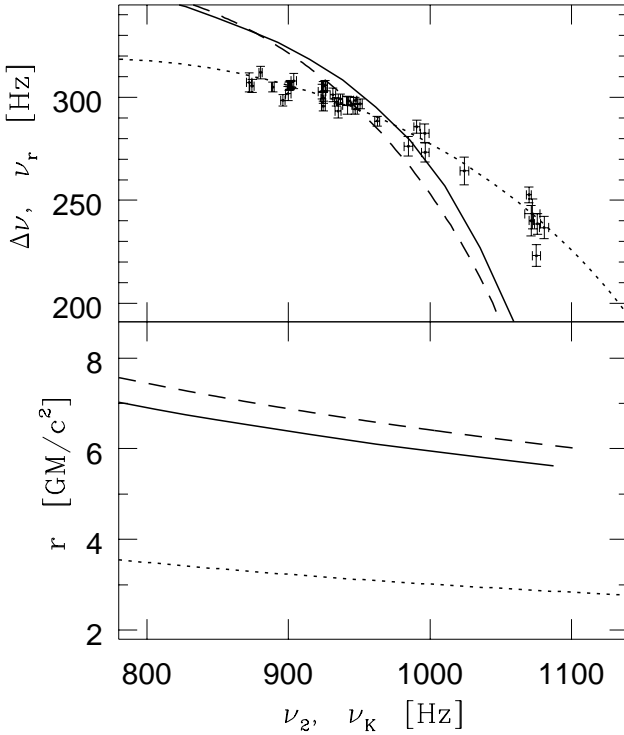


Figure 1. *Upper panel:* ν_r - ν_K relations given by two sequences of infinitesimally eccentric geodesics that best fit the ν_1 and ν_2 data for the Z source Sco X-1. The dashed curve shows the ν_r - ν_K relation given by the best-fitting geodesic sequence around a non-rotating star ($M = 1.99 M_\odot$; $\chi^2/\text{dof} = 38$). The solid curve shows the relation given by the best-fitting geodesic sequence around a rotating star constructed using the UU EOS ($M = 2.21 M_\odot$, $\nu_s = 450$ Hz; $\chi^2/\text{dof} = 35$); the relation given by the best-fitting geodesic sequence around a rotating star constructed using EOS L is almost identical. The dotted curve shows the ν_r - ν_K relation given by the best-fitting sequence of geodesics around a black hole ($M = 5.8 M_\odot$, $j = 0.89$; $\chi^2/\text{dof} = 1.6$). *Lower panel:* Circumferential radii of the geodesics that give the frequencies plotted in the upper panel.

3.1 Frequencies of infinitesimally and moderately eccentric geodesics

The most numerous and precise kilohertz QPO frequency measurements are those for the Z source Sco X-1 (van der Klis et al. 1997). We therefore consider consistency with the frequency correlation observed in this source as a necessary condition for any QPO model to be viable (a very similar correlation has been observed in 4U 1608–52; see Méndez et al. 1998). The frequency relations given by geodesics around nonrotating stars provide useful guidance because the ν_r - ν_K relation is relatively insensitive to the stellar spin rate and the relation for a nonrotating star doesn't depend on the EOS of neutron star matter, provided that it is hard enough to support the stellar mass being considered and gives stars with $R_e < r_{a,\min}$). Only geodesics near r_{isco} are relevant, because ν_r decreases appreciably with increasing ν_K only near r_{isco} .

The dashed curve in Fig. 1 shows the frequency relation constructed from IEGs around a nonrotating star that best fits the Sco X-1 data; the stellar mass derived from this fit is $1.99 M_\odot$, which is a reasonable mass for a neutron star in an

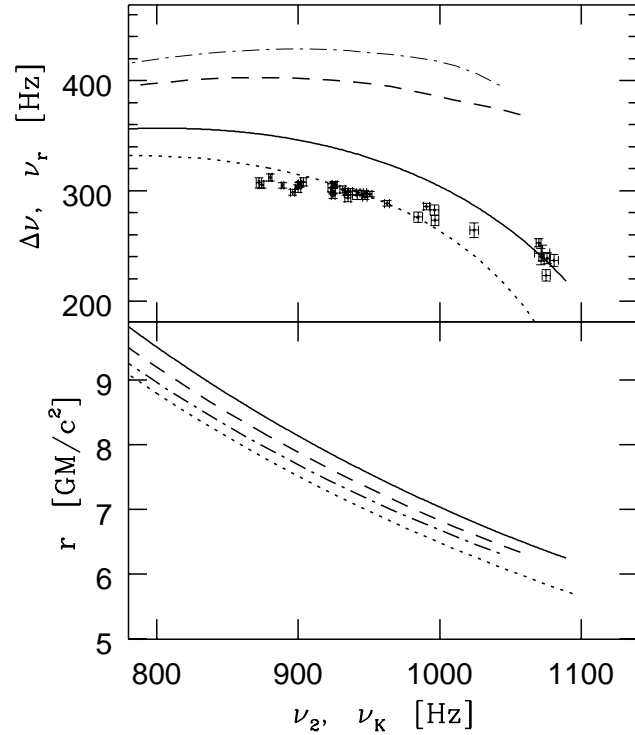


Figure 2. *Upper panel:* Comparison of the ν_r - ν_K relations discussed in the text with measurements of $\Delta\nu$ and ν_2 in Sco X-1. The solid curve shows the ν_r - ν_K relation given by the geodesic sequence around a nonrotating star that SV reported as fitting the Sco X-1 data; χ^2/dof for this sequence is 150. The dashed and dash-dotted curves show the ν_r - ν_K relations given by the geodesic sequences around the stars with spin rates of 300 Hz and 600 Hz that SV also reported as fitting the Sco X-1 data. The dotted curve shows the ν_r - ν_K relation given by the sequence of geodesics around a rotating UU star with $r_p \geq r_{isco}$ but any value of r_a ($\geq r_p$) that best fits the ν_1 and ν_2 data for Sco X-1 ($M = 2.21 M_\odot$, $\nu_s = 450$ Hz, $r_p = r_{isco} = 5.52$; $\chi^2/\text{dof} = 21$). *Lower panel:* Circumferential apastron radii of the geodesics that give the frequencies plotted in the upper panel.

LMXB. The dashed curve is very similar to the curve shown in Fig. 1 of SV for IEGs around a nonrotating star with a mass of $2.0 M_\odot$. As Fig. 1 shows, the frequency relation for the best-fitting sequence of IEGs around a nonrotating star is much steeper than the observed frequency correlation; the qualitative disagreement between the best-fitting frequency relation and the frequency data is indicated by the large χ^2/dof for this fit, which is 38.

As noted by SV, stellar rotation has little effect on the relation between ν_{AP} and ν_K . This is illustrated in Fig. 1 by the similarity of the frequency relation for the rotating star constructed using the UU EOS that best fits the Sco X-1 data to the relation for the nonrotating star that fits best. The frequency relation for the rotating star constructed using EOS L that best fits the data is also very similar to the relation for the nonrotating star that fits best. Although prograde spin does decrease slightly the slope of the predicted ν_r - ν_K relation for a given mass, the effect is small. The reason is that the dragging of inertial frames causes r_{isco} to decrease, which significantly increases the azimuthal frequency of geodesics near r_{isco} for a given stellar mass. Hence

the mass of the star must be increased in order to keep the azimuthal frequencies in the observed range (all frequencies scale approximately as $1/M$). This drives the stellar mass close to the maximum mass allowed by the EOS. Indeed, the mass of a rotating UU star that fits best is $2.21 M_\odot$, which is the maximum stable mass for this EOS and the best-fitting spin rate (450 Hz). The χ^2/dof for this fit is 35.5, only slightly smaller than the χ^2/dof for the nonrotating star that fits best. The fit is not any better for harder equations of state. Although they give larger maximum masses, ν_r falls more steeply because of their larger size and hence larger quadrupolar deformation (Marković 2000).

SV argued that ν_{AP} and ν_{K} would agree with the observed frequencies of the kilohertz QPOs if clumps form on MEGs rather than IEGs. To support their argument, they showed in their Fig. 2 a frequency relation supposedly for a sequence of MEGs with $r_p = 6.25M$ around a $M = 1.9 M_\odot$ nonrotating star; this relation appears to agree fairly well with the Sco X-1 frequency data. However, as explained in detail in the Appendix, the ν_r - ν_{K} relation plotted by SV was computed incorrectly. The solid curve in Fig. 2 shows the actual ν_r - ν_{K} relation for the sequence of MEGs specified by SV. It is similar to the relation for the best-fitting sequence of IEGs and is much steeper than the data ($\chi^2/\text{dof} = 150$).

SV also reported that sequences of MEGs with $r_p \approx 6.18M$ and $6.17M$ around rotating neutron stars with masses of $1.94 M_\odot$ and $1.98 M_\odot$ constructed using EOS L with, respectively, $\nu_s = 300$ Hz and 600 Hz also give ν_r - ν_{K} relations similar to the $\Delta\nu$ - ν_2 correlation observed in Sco X-1. We have computed the ν_r - ν_{K} relations for these geodesic sequences. The results are shown as the dashed and dashed-dotted curves in Fig. 2; these curves lie 100–200 Hz above the Sco X-1 frequency correlation.

The dotted curve in Fig. 2 shows the frequency relation for the best-fitting sequence of geodesics around a rotating star constructed using geodesics that meet the requirement $r_p \geq r_{\text{isco}}$ proposed by SV but are otherwise unrestricted. With this freedom, the low-frequency geodesics become more eccentric ($r_{\text{a,max}}/r_p \approx 1.5$), but the frequency relation remains much steeper than the data ($\chi^2/\text{dof} = 21$). For the reasons discussed above, the stellar mass that fits best is equal to the maximum mass for the best-fit spin rate.

The frequency relations for sequences of MEGs around stars constructed using other equations of state are also inconsistent with the Sco X-1 data. The frequency relations given by sequences of IEGs and MEGs also disagree with the kilohertz QPO frequencies of other sources, although frequency measurements for sources other than Sco X-1 are sparser and less precise. For example, the best-fitting sequence of MEGs with $r_p \geq r_{\text{isco}}$ around a UU star with the 363 Hz spin rate inferred from the burst oscillations of 4U 1728–34 (Strohmayer et al. 1996; Méndez & van der Klis 1999) has $M = 1.92 M_\odot$ and gives $\chi^2/\text{dof} \approx 15$. If instead the stellar spin rate is treated as a free parameter, the best-fitting MEG sequence with $r_p \geq r_{\text{isco}}$ has $\nu_s \approx 900$ Hz and $M = 2.20 M_\odot$ and gives $\chi^2/\text{dof} = 9.4$. This mass is again very close to the maximum stable mass for this EOS.

Almost all the best-fitting neutron star masses given by MEG sequences are very close to the maximum stable mass for the assumed EOS, which is implausible. More seriously, the ν_r - ν_{K} relations given by sequences of MEGs devi-

ate by large fractional amounts ($\Delta\nu_r/\nu_r$ as much as 30% or $\Delta\nu_{\text{K}}/\nu_{\text{K}}$ as much as 15%) from the $\Delta\nu$ - ν_2 correlations observed. Any forces strong enough to bring these frequency relations into agreement with the data would invalidate the geodesic motion hypothesis.

Fig. 1 shows that one can construct a sequence of IEGs around a $5.8 M_\odot$, rapidly spinning ($j = 0.89$) black hole that gives a frequency relation which agrees fairly well with the kilohertz QPO frequencies observed in Sco X-1 ($\chi^2/\text{dof} = 1.6$). There is compelling evidence that Sco X-1 is not a black hole (see, e.g., van der Klis 2000). The fairly good agreement of IEGs in the Kerr spacetime with the Sco X-1 frequency data is a reminder that successfully fitting QPO frequencies does not by itself validate a model. The wealth of other information that is available about the kilohertz QPOs and the kilohertz QPO sources must also be taken into account.

These results show that regardless of the neutron star model and spin rate assumed, the MEG hypothesis gives frequency relations that are qualitatively different from the observed correlations between the kilohertz QPO frequencies. As explaining this correlation was the primary motivation for introducing the MEG hypothesis (SV), we consider this failure serious enough to set aside the MEG hypothesis and we therefore do not consider it further.

3.2 Frequencies of highly eccentric geodesics

We consider now whether allowing highly eccentric geodesics (HEGs) would make it possible to construct sequences that give values of ν_{AP} and ν_{K} consistent with the values of ν_1 and ν_2 observed in the kilohertz QPO sources. As before, we assume that the periastron radius r_p has a constant value $> R_e$, if there is no marginally bound geodesic, or $> r_{\text{mb}}$, but we allow the apastron radius r_a to have any value $> r_p$.

3.2.1 Sco X-1 kilohertz QPO frequencies

Fig. 3 shows the ν_{AP} - ν_{K} relations given by the sequences of geodesics around stars constructed using EOS UU and EOS C that fit best the ν_1 and ν_2 data for Sco X-1.

The best-fitting sequence for stars constructed using the UU EOS is for a nonrotating star with $M = 1.89 M_\odot$. This fit gives $\chi^2/\text{dof} = 1.4$, which is unacceptable at the 94% confidence level. To achieve fits this good, the sequence must include HEGs with $r_a/r_p = 2.1$. Such highly eccentric geodesics are required in order to generate ν_r - ν_{K} relations that are sufficiently flat. Physically, clumps must be formed or injected on a special sequence of highly eccentric geodesics with a common periastron radius that is 40% larger than the stellar radius and 15% smaller than r_{isco} (as shown in Fig. 2, if $r_p > r_{\text{isco}}$ is required, as suggested by SV, the fits would be much poorer). The best-fitting mass is about $0.3 M_\odot$ less than the maximum stable mass and hence the fit is relatively insensitive to the stellar spin rate (χ^2/dof would be about the same for any spin frequency $\lesssim 600$ Hz). This geodesic sequence is the best-fitting sequence for any EOS that can support a nonrotating star with $M > 1.89 M_\odot$ and an equatorial radius $R_e < 5.3M$.

The best-fitting geodesic sequence for stars constructed using the softer EOS C is for a nonrotating star with $M = 1.86 M_\odot$, the maximum stable mass for this EOS. The

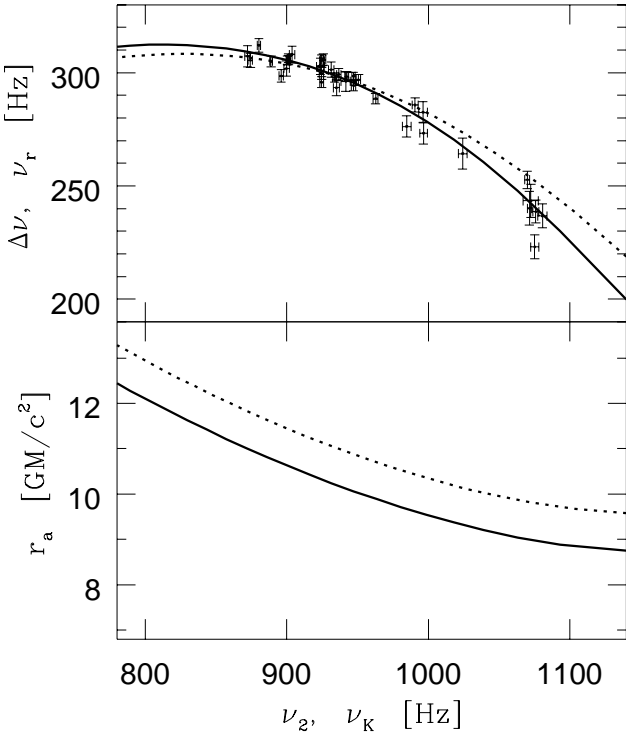


Figure 3. *Upper panel:* ν_r - ν_K relations given by two geodesic sequences that best fit the ν_1 and ν_2 data for Sco X-1. The solid curve shows the ν_r - ν_K relation given by the geodesic sequence that fits best overall ($M = 1.89 M_\odot$, $\nu_s = 0$, $r_p = 5.3M$; $\chi^2/\text{dof} = 1.4$). This is the best-fitting sequence for any EOS, such as UU, that can support a nonrotating star with $M > 1.89 M_\odot$ and an equatorial radius $R_e < 5.3M$. The dotted curve shows the ν_r - ν_K relation given by the best-fitting sequence for EOS C ($M = 1.86 M_\odot$, $\nu_s = 0$, $r_p = 5.1M$; $\chi^2/\text{dof} = 2.2$); the fit would be worse for a rotating star (see text). To achieve fits this good, both sequences must include highly eccentric geodesics. *Lower panel:* Circumferential apastron radii of the highly eccentric geodesics that give the frequencies displayed in the upper panel.

smaller maximum mass of C stars requires geodesics that are more eccentric than for UU stars, in order to keep ν_r within the observed range of $\Delta\nu$. This causes the slope of the best-fitting ν_r - ν_K relation to be flatter than for UU stars and flatter than the observed correlation ($\chi^2/\text{dof} = 2.2$). Requiring the star to have a spin rate $\gtrsim 300$ Hz, like that expected for the neutron stars in the kilohertz QPO sources, would increase all orbital frequencies, making the fit significantly worse (the maximum mass is not increased significantly for the relevant spin rates). We conclude that the geodesic precession hypothesis is inconsistent with the kilohertz QPO frequencies observed in Sco X-1 if neutron star matter is as soft as EOS C.

3.2.2 GX 340+0 kilohertz QPO frequencies

Fig. 4 shows the ν_r - ν_K relations given by the sequences of geodesics for neutron stars constructed using EOS C and EOS UU that best fit the ν_1 and ν_2 data for the Z source GX 340+0 (Jonker et al. 1998). The fit is again better for higher mass stars, because the observed frequencies of the upper kilohertz QPO in GX 340+0 are relatively low when

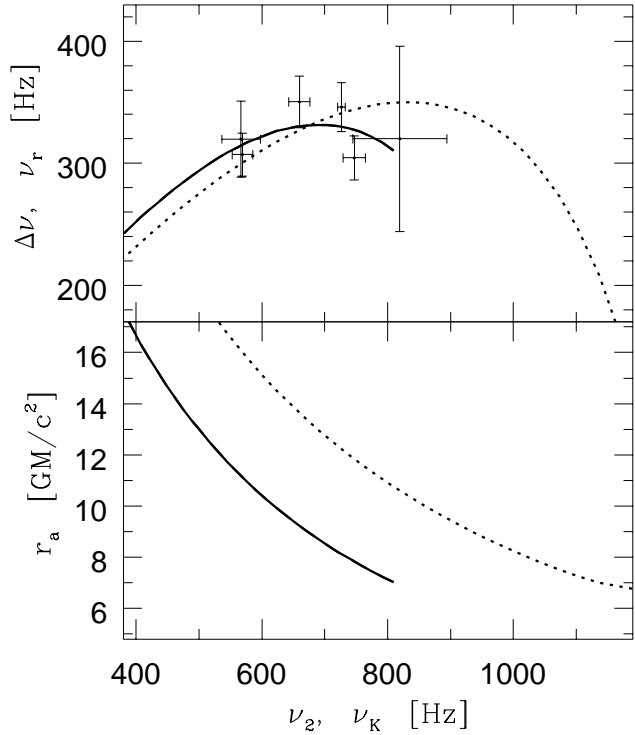


Figure 4. *Upper panel:* ν_r - ν_K relations given by two geodesic sequences that best fit the ν_1 and ν_2 data for the Z source GX 340+0. The solid and dotted curves show respectively the ν_r - ν_K relations given by the best-fitting sequences for neutron stars constructed using EOS UU ($M = 2.12 M_\odot$, $\nu_s = 0$, $r_p = 7.0M$; $\chi^2/\text{dof} = 0.84$) and EOS C ($M = 1.86 M_\odot$, $\nu_s = 0$, $r_p = 5.8M$; $\chi^2/\text{dof} = 2.3$). Both sequences require highly eccentric geodesics ($r_{a,\text{max}}/r_p = 1.6\text{--}2.8$). *Lower panel:* Circumferential apastron radii of the highly eccentric geodesics that give the frequencies displayed in the upper panel.

interpreted as azimuthal frequencies near the ISCO. Hence stars constructed using EOS C fit significantly worse than stars constructed using EOS UU, because the former have smaller maximum stable masses.

The best-fitting geodesic sequence for stars constructed using EOS C is for a nonrotating star with a mass equal to the maximum stable mass for this EOS, requires a very high eccentricity ($r_{a,\text{max}}/r_p = 2.8$), and does not fit the data adequately ($\chi^2/\text{dof} = 2.3$), even though the uncertainties in the measured frequency differences $\Delta\nu$ are rather large. The disagreement would be worse for a rotating star. Hence we conclude that the geodesic precession hypothesis is inconsistent with the kilohertz QPO frequency correlation observed in GX 340+0 if neutron star matter is as soft as EOS C. We caution, however, that a better understanding of the uncertainties in measurements of ν_2 above 700 Hz caused by the higher noise power density at these frequencies (Jonker et al. 1998) could affect this conclusion.

The best-fitting geodesic sequence for the UU EOS again requires highly eccentric ($r_{a,\text{max}}/r_p = 1.6$) geodesics with a fixed periastron radius more than twice as large as the star's equatorial radius. The sequence of geodesics around a nonrotating star that fits best has a mass only about $0.1 M_\odot$ less than the maximum stable mass for this EOS; χ^2/dof for the best-fitting sequence is 0.84. The best-fitting geodesic se-

quence and the χ^2/dof would be approximately the same for any spin rate $\lesssim 200$ Hz.

3.2.3 4U 1728–34 kilohertz QPO frequencies

The observed frequencies of the kilohertz QPOs in the atoll source 4U 1728–34 narrow further the range of equations of state consistent with the geodesic precession hypothesis. Fig. 5 shows the $\nu_r - \nu_K$ relation given by the sequence of geodesics for stars constructed using the UU EOS that best fit the ν_1 and ν_2 data for 4U 1728–34. This fit assumes that the stellar spin frequency is the 363 Hz frequency of the burst oscillations in this source. The fit would be very similar for any spin frequency $\lesssim 500$ Hz.

Again, a $\nu_r - \nu_K$ relation qualitatively similar to the observed $\nu_1 - \nu_2$ correlation can be achieved only by using HEGs. The $\nu_r - \nu_K$ relation given by the best-fitting geodesic sequence for stars constructed using the UU EOS has $r_{a,\text{max}}/r_p = 2.7$ and gives $\chi^2/\text{dof} = 1.7$. The large scatter in the observed $\Delta\nu - \nu_2$ relation for upper kilohertz QPO frequencies in the range $1150 \lesssim \nu_2 \lesssim 1200$ Hz (see Méndez & van der Klis 1999) contributes significantly to the χ^2/dof . This scatter appears inconsistent with the simple, smooth frequency relations characteristic of geodesic precession models. The best-fitting geodesic sequence for stars constructed using the modern, realistic EOS A18+UIX+ δv_b gives the same model parameters, except that the best-fitting value of r_p is $1.05R_e$ instead of $1.09R_e$ (see Table 3 below).

Stars constructed using harder equations of state, such as the early EOS L, which are now thought to be unrealistically hard, have larger maximum masses but also larger equatorial radii. This eliminates some of the highly eccentric geodesics that are available if the EOS is softer, making the geodesic precession hypothesis inconsistent with the kilohertz QPO data for such hard equations of state. The 4U 1728–34 frequency data illustrate this. The flatness of the $\Delta\nu - \nu_K$ correlation for $\nu_2 \lesssim 1100$ Hz (see Fig. 5) constrains the mass of the neutron star to be $\lesssim 2M_\odot$. The large equatorial radii of stars constructed using hard equations of state leave room only for less highly eccentric geodesics, which produce $\nu_r - \nu_K$ relations that fall steeply at high ν_K and are therefore inconsistent with the observed $\Delta\nu - \nu_2$ correlation.

Our findings up to this point show that $\nu_{\text{AP}} - \nu_K$ relations similar to the $\nu_1 - \nu_2$ correlations observed in the kilohertz QPO sources require highly eccentric geodesics and are not possible for geodesics around neutron stars constructed with equations of state that are either significantly softer or significantly harder than the UU EOS, i.e., the geodesic precession hypothesis is inconsistent with softer or harder equations of state. Hence, from now on we consider only EOS UU. The realistic modern EOS A18+UIX+ δv_b gives results that differ only very slightly from those obtained with the UU EOS.

3.2.4 GX 5–1 and GX 17+2 kilohertz QPO frequencies

Fig. 6 shows the ten pairs of kilohertz QPO frequencies measured so far in the Z source GX 5–1 (Wijnands et al. 1998). Most have relatively large uncertainties and one (the circled point in the figure) appears discordant. If all ten frequency pairs are included, the $\nu_r - \nu_K$ relation given by the

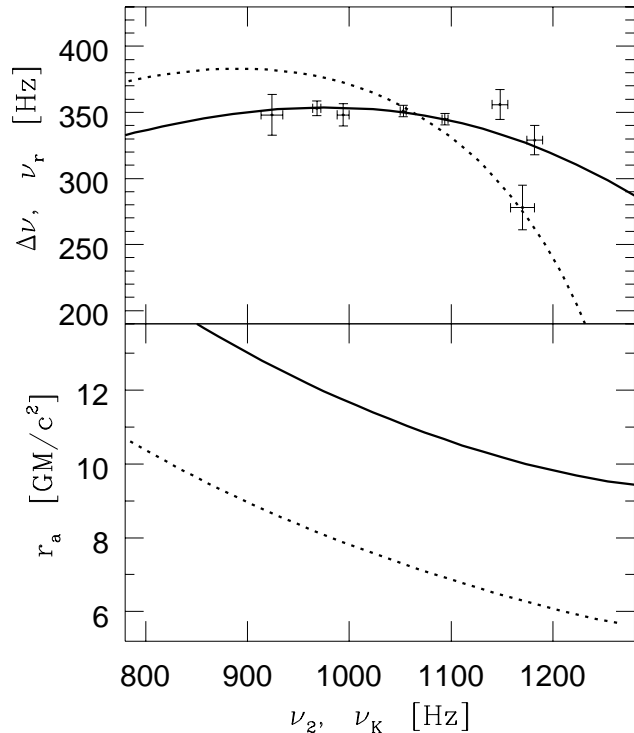


Figure 5. *Upper panel:* $\nu_r - \nu_K$ relations given by two geodesic sequences that best fit the $\nu_1 - \nu_2$ data for the atoll source 4U 1728–34. The solid and dotted curves show respectively the $\nu_r - \nu_K$ relations given by the best-fitting sequences for neutron stars constructed using EOS UU ($M = 1.76 M_\odot$, $r_p = 4.7M = 1.09R_e = 12.4$ km; $\chi^2/\text{dof} = 1.7$) and EOS L ($M = 1.97 M_\odot$, $r_p = R_e = 5.3M = 15.4$ km; $\chi^2/\text{dof} = 8.6$), assuming $\nu_s = 363$ Hz, the burst oscillation frequency. Both sequences require highly eccentric geodesics ($r_{a,\text{max}}/r_p = 2.7$ for the best-fitting UU sequence). *Lower panel:* Circumferential apastron radii of the highly eccentric geodesics that give the frequencies displayed in the upper panel.

best-fitting sequence of geodesics for stars constructed using EOS UU has a rather large χ^2/dof ; discarding the discordant frequency pair gives a smaller χ^2/dof of 1.2. However, values of χ^2/dof this small are possible only if the star has a mass $M \approx 2.1$ – $2.2 M_\odot$ near the maximum stable mass and highly eccentric geodesics are included ($r_{a,\text{max}}/r_p \approx 2.1$).

Only eight pairs of kilohertz QPO frequencies have been measured so far in the Z source GX 17+2 (Wijnands et al. 1997; see Fig. 11 below). The $\nu_r - \nu_K$ relation given by the best-fitting sequence of geodesics for stars constructed using EOS UU is acceptable ($\chi^2/\text{dof} \approx 0.4$), but only if all the geodesics are highly eccentric ($r_{a,\text{max}}/r_p \approx 3$ – 4). However, the uncertainties in these frequency measurements are large.

3.3 Other geodesic frequencies

We have also explored whether the frequencies of the two kilohertz QPOs are consistent with geodesic frequencies other than ν_{AP} and ν_K . As discussed in Section 4, the most prominent frequencies generated by clumps moving on geodesics around neutron stars are ν_r , $2\nu_r$, $\nu_K + \nu_r$, and $\nu_K + 2\nu_r$. We find that for realistic neutron star models, these frequencies are not in the same range as the frequencies of

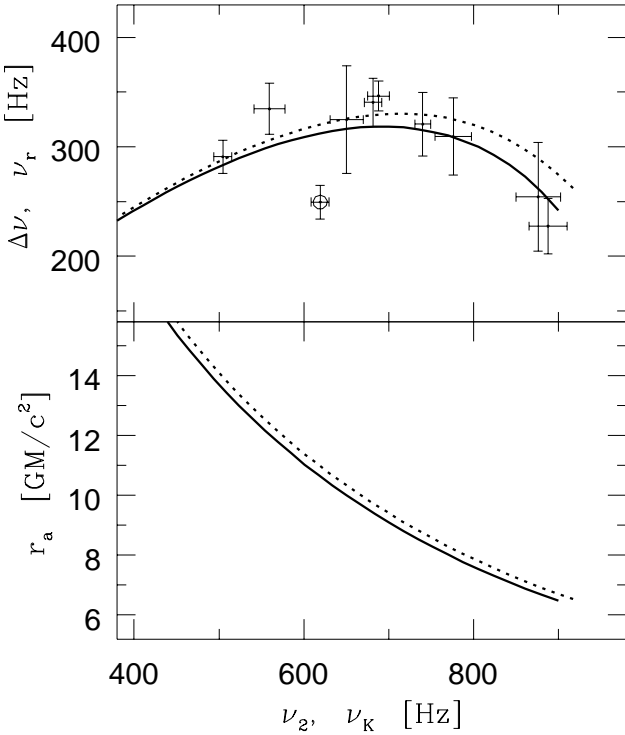


Figure 6. *Upper panel:* ν_r - ν_K relations given by two geodesic sequences that best fit the ν_1 - ν_2 data for the Z source GX 5–1. The solid and dotted curves show respectively the ν_r - ν_K relations given by the best-fitting sequences for neutron stars constructed using the UU EOS if all the frequency measurements are included ($M = 2.17 M_\odot$, $r_p = 6.5M$; $\chi^2/\text{dof} = 3.6$) or, alternatively, if all but the circled measurement are included ($M = 2.09 M_\odot$, $r_p = 6.5M$; $\chi^2/\text{dof} = 1.2$). Fits this good require highly eccentric geodesics with $r_a/r_p \approx 2$. *Lower panel:* Circumferential apastron radii of the highly eccentric geodesics that give the frequencies displayed in the upper panel.

the kilohertz QPOs. The two frequencies ν_K and $\nu_K + \nu_r$ are in the same range as the frequencies of the kilohertz QPOs only for unrealistically hard neutron-star equations of state, such as EOS L; however, even for such hard equations of state, the best-fitting geodesic sequences give frequency relations that have qualitatively different shapes from those observed and give $\chi^2/\text{dof} > 10$ for GX 340+0 and GX 5–1. We therefore conclude that geodesic frequencies other than ν_{AP} and ν_K are not viable explanations of the frequencies of the kilohertz QPOs.

3.4 LFQPO and HBO frequencies

In the previous two sections we investigated whether sequences of geodesics can be found that give ν_{AP} - ν_K relations consistent with the kilohertz QPO frequencies observed in the Z and atoll sources. There we showed that the best-fitting sequences of infinitesimally or moderately eccentric geodesics give ν_{AP} - ν_K relations qualitatively different from the kilohertz QPO frequency correlations in all the sources considered. We showed further that ν_{AP} - ν_K relations similar to the kilohertz QPO frequencies observed in the sources considered are possible only if highly eccentric geodesics ($r_a/r_p \sim 2$ –4) are included in all the sequences. HEG se-

quences can be found that give ν_{AP} - ν_K relations roughly consistent with the ν_1 - ν_2 correlations observed in Sco X-1 and 4U 1728–34, although the values of χ^2/dof are not formally acceptable. HEG sequences can also be found that formally fit the ν_1 - ν_2 correlations observed in GX 17+2 and GX 340+0, but there are only a few frequency measurements for each these sources and the uncertainties are large. However, the geodesic sequence that best fits the GX 5–1 frequency data appears to be inconsistent with these data.

SV and SVM proposed that gas orbits the neutron stars in the Z and atoll sources in the form of clumps moving on slightly inclined geodesics and that the low-frequency peaks observed in power spectra of the Z and atoll sources are caused by nodal precession of these geodesics. As explained in Section 1, ν_{NP} is too low to explain the frequencies of these low-frequency features. SV and SVM therefore suggested that clump nodal precession somehow produces an X-ray oscillation with frequency $2\nu_{\text{NP}}$. (However, as explained in Section 4, we were unable to find a clump mechanism that generates a significant peak at $2\nu_{\text{NP}}$.)

Here we follow up the proposal that the low-frequency peaks are generated by nodal precession by investigating whether sequences of geodesics can be found that give ν_{AP} - ν_K and $2\nu_{\text{NP}}$ - ν_K relations that are both *simultaneously* consistent with the ν_L - ν_2 and ν_1 - ν_2 correlations observed in the Z and atoll sources. In contrast to the ν_{AP} - ν_K relations studied in the previous section, the $2\nu_{\text{NP}}$ - ν_K relations studied here are sensitive to the stellar spin rate, because of the gravitomagnetic effect.

Before proceeding, we caution that measurements of the centroid frequencies of the bumps observed in atoll-source power spectra can be affected significantly by systematic errors that arise from uncertainties in modeling the noise continuum in the vicinity of these features (M. Méndez and M. van der Klis 1999, private communication). The systematic errors are often difficult to estimate and typically are not reported in the literature. Instead, only statistical errors are reported. We use the reported errors to make a preliminary assessment of whether the fits below are acceptable, but one should bear in mind that the total errors may be somewhat larger.

3.4.1 4U 1728–34 LFQPO and kilohertz QPO frequencies

The $2\nu_{\text{NP}}$ - ν_K relation given by the geodesic sequence which gives the ν_{AP} - ν_K relation that best fits the ν_1 - ν_2 data in 4U 1728–34 (see Section 3.2 and Fig. 5) has a shape that is qualitatively different from the observed ν_L - ν_K correlation in this source (see Fig. 7). The predicted relation shown is for a stellar model constructed using the UU EOS and a spin rate equal the 363 Hz burst oscillation frequency. The fit cannot be improved significantly by increasing or decreasing the spin rate.

We also considered stellar models constructed using the modern realistic EOS A18+UIX+ δv_b (see Section 2.1). The best-fitting stellar mass is 0.1% larger and the dimensionless angular momentum is 3% larger ($j = 0.156$ vs. $j = 0.149$) for this EOS, because it is slightly harder. This increases the nodal precession frequency for geodesics with a given ν_K , but only by $\lesssim 4\%$.

The predicted $2\nu_{\text{NP}}$ - ν_K relation shown in Fig. 7 is clearly inconsistent with the observed ν_L - ν_2 correlation: the pre-

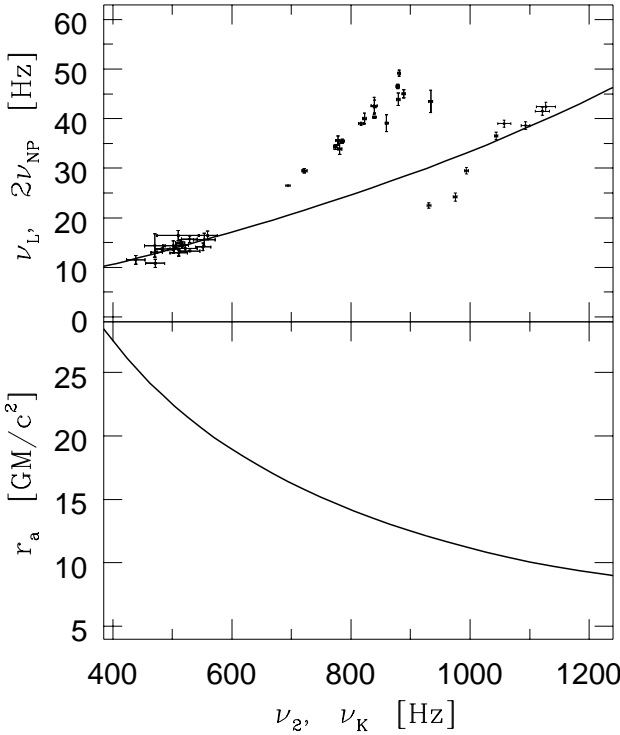


Figure 7. *Upper panel:* Comparison of the ν_L - ν_K behaviour seen in 4U 1728–34 with the $2\nu_{NP}$ - ν_K relation predicted by the geodesic sequence that gives the best fit to the ν_1 - ν_2 data for this source (see Fig. 5). *Lower panel:* Circumferential apastron radii of the highly eccentric geodesics that give the frequencies displayed in the upper panel.

dicted relation does not reproduce the abrupt drop in ν_L by a factor > 2 that occurs at $\nu_2 \approx 900$ Hz in the observed correlation, nor is it consistent with the observed ν_L - ν_2 correlation either before or after the abrupt drop. The predicted ν_{NP} - ν_K relation misses many of the observed values of ν_L by a factor ~ 2 . This qualitative disagreement between the frequency behavior predicted by the nodal precession hypothesis and the frequency behaviour observed in 4U 1728–34 occurs for any realistic neutron star model and spin rate.

Very recent analyses of 4U 1728–34 power spectra (Di Salvo et al. 2000, private communication) indicate that the break frequency of the low-frequency broad-band noise component and the frequency of the LFQPO are related: the frequencies of the break and the LFQPO both increase as the frequency of the upper kilohertz QPO increases from 400 to 900 Hz, but at this point the existing LFQPO disappears and the noise feature peaks up into a new LFQPO. The frequency of the old and new LFQPOs are not harmonically related. This behaviour appears inconsistent with any simple interpretation in terms of nodal precession of HEGs.

3.4.2 GX 5–1 HBO and kilohertz QPO frequencies

The behaviour of $2\nu_{NP}$ is also qualitatively inconsistent with the behaviour of the HBO frequency in GX 5–1. This is illustrated in Fig. 8, which compares the ν_{HBO} - ν_2 correlation observed in GX 5–1 with the $2\nu_{NP}$ - ν_K relations predicted

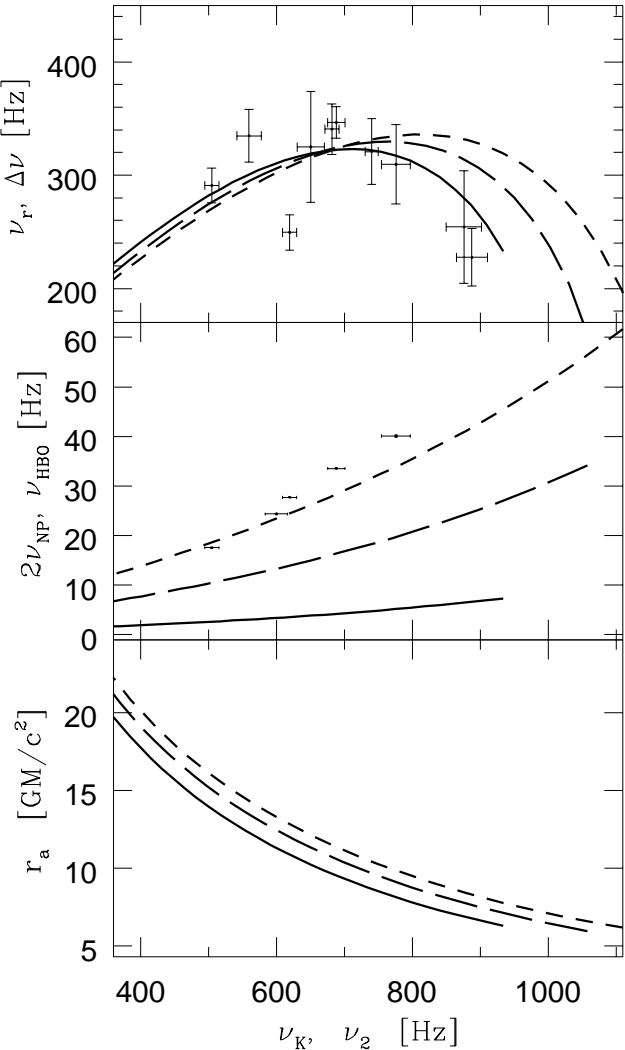


Figure 8. Geodesic sequences around UU stars that best fit the ν_1 - ν_2 data for GX 5–1, for different stellar spin rates. The solid, long-dashed, and short-dashed curves show the relations given by the geodesic sequences that fit best for $\nu_s = 100$ Hz ($M = 2.20 M_\odot$, $r_p = 6.3M$; $\chi^2/\text{dof} = 3.6$), $\nu_s = 363$ Hz ($M = 2.21 M_\odot$, $r_p = 5.8M$; $\chi^2/\text{dof} = 4.5$) and $\nu_s = 600$ Hz ($M = 2.22 M_\odot$, $r_p = 5.3M$; $\chi^2/\text{dof} = 5.6$). $R_e = 3.02M$ for all three stellar models. *Top panel:* Comparison of the best-fitting ν_{AP} - ν_K relations with the observed ν_1 - ν_2 correlation. *Middle panel:* Comparison of the predicted ν_{NP} - ν_K relations with the observed ν_{HBO} - ν_2 correlation. *Bottom panel:* Circumferential apastron radii of the highly eccentric geodesics that give the frequencies plotted in the upper and middle panels.

by several geodesic sequences constructed to give ν_{AP} - ν_K relations that fit as well as possible the ν_1 - ν_2 data.

The basic difficulty is that in order to construct a sequence of HEGs that gives a ν_{AP} - ν_K relation similar to the observed ν_1 - ν_2 correlation, the stellar spin rate must be $\lesssim 400$ Hz, but for spin rates this low, $2\nu_{NP}$ is much smaller than the observed HBO frequencies. If the spin rate is increased to the values $\gtrsim 600$ Hz required to lift $2\nu_{NP}$ into the observed frequency range of the HBO, ν_K is shifted upward so much that the ν_{AP} - ν_K relation given by the best-fitting geodesic sequence is much flatter than the observed ν_{HBO} - ν_K correlation. Furthermore, attempting to fit this correlation

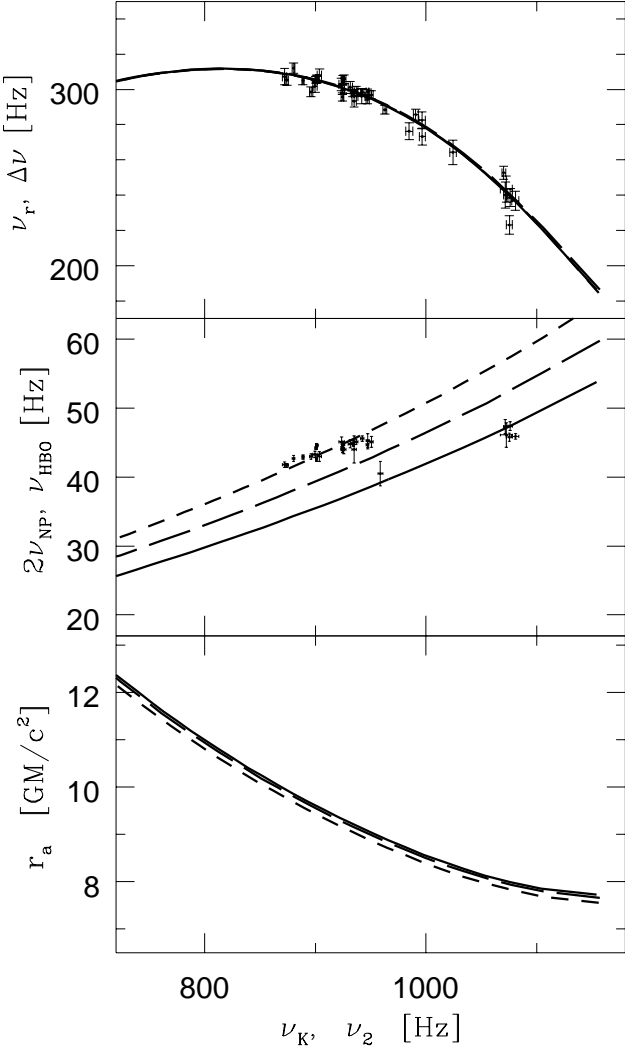


Figure 9. Geodesic sequences around UU stars that best fit the $\nu_1-\nu_2$ data for Sco X-1, for different stellar spin rates. The solid, long-dashed, and short-dashed curves show the relations given by the geodesic sequences that fit best for $\nu_s = 450$ Hz ($M = 2.13 M_\odot$, $R_e = 3.32 M$, $r_p = 4.9 M$), $\nu_s = 500$ Hz ($M = 2.16 M_\odot$, $R_e = 3.27 M$, $r_p = 4.8 M$) and $\nu_s = 550$ Hz ($M = 2.18 M_\odot$, $R_e = 3.19 M$, $r_p = 4.8 M$). $\chi^2/\text{dof} = 1.4$ for all three sequences. *Top panel:* Comparison of the best-fitting $\nu_{\text{AP}}-\nu_K$ relations with the observed $\nu_1-\nu_2$ correlation. *Middle panel:* Comparison of the predicted $2\nu_{\text{NP}}-\nu_K$ relations with the observed $\nu_{\text{HBO}}-\nu_2$ correlation. *Bottom panel:* Circumferential apastron radii of the highly eccentric geodesics that give the frequencies plotted in the upper and middle panels.

drives the stellar mass to the maximum stable mass for the spin rate considered, which is implausible.

3.4.3 Sco X-1 HBO and kilohertz QPO frequencies

The behaviour of $2\nu_{\text{NP}}$ is qualitatively inconsistent with the observed behaviour of the HBO frequency in Sco X-1. This is demonstrated in Fig. 9, which compares the $\nu_{\text{HBO}}-\nu_2$ correlation observed in Sco X-1 with the $2\nu_{\text{NP}}-\nu_K$ relations predicted by three sequences of HEGs constructed to give the $\nu_{\text{AP}}-\nu_K$ relation that best fits the $\nu_1-\nu_2$ data for Sco X-1, for

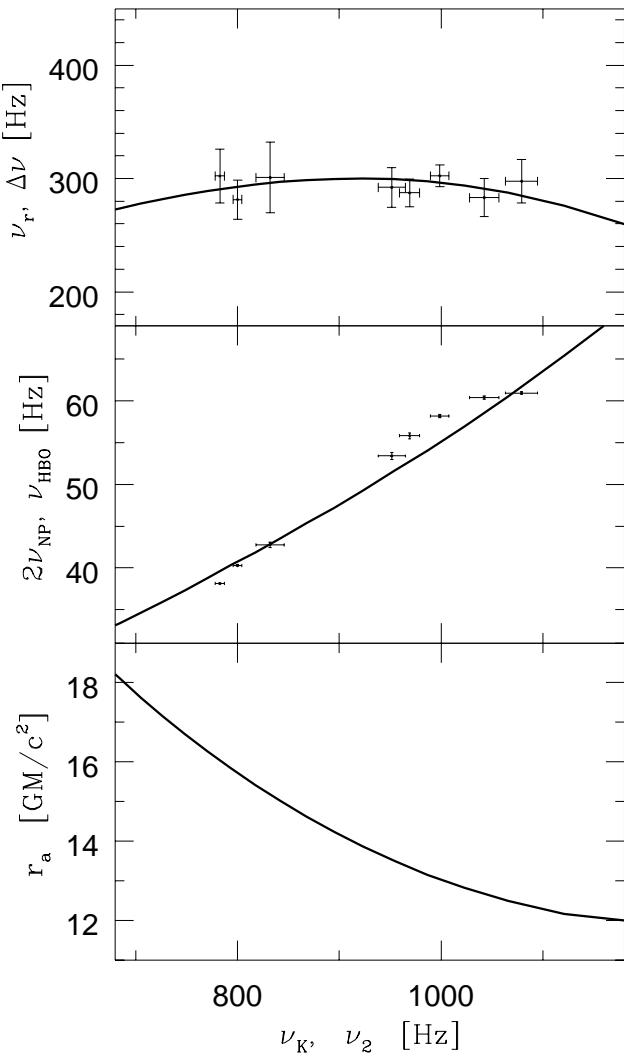


Figure 10. The geodesic sequence around UU stars that best fits the $\nu_1-\nu_2$ data for GX 17+2. The best-fit parameters are $M = 1.82 M_\odot$ and $r_p = 4.2 M \approx 1.01 R_e$; $\chi^2/\text{dof} = 0.39$. *Top panel:* Comparison of the best-fitting $\nu_r-\nu_K$ relation with the observed $\Delta\nu-\nu_2$ correlation. *Middle panel:* Comparison of the predicted $2\nu_{\text{NP}}-\nu_K$ relation with the observed $\nu_{\text{HBO}}-\nu_2$ correlation, for $\nu_s = 550$ Hz. *Bottom panel:* Circumferential apastron radii of the highly eccentric geodesics that give the frequencies plotted in the upper and middle panels.

various assumed spin rates. For the reason discussed previously, the predicted $\nu_{\text{AP}}-\nu_K$ relations are insensitive to the star's spin frequency for the frequencies considered and they therefore lie almost on top of one another.

Here the basic difficulty is that the $2\nu_{\text{NP}}-\nu_K$ relations predicted by the geodesic sequences that give acceptable fits to the $\nu_1-\nu_2$ data rise much more steeply than the observed $\nu_{\text{HBO}}-\nu_2$ correlation, regardless of the spin rate of the star.

3.4.4 GX 17+2 HBO and kilohertz QPO frequencies

The behaviour of $2\nu_{\text{NP}}$ predicted by the sequence of HEGs that best fits the $\nu_1-\nu_2$ data for GX 17+2 is qualitatively similar to the $\nu_{\text{HBO}}-\nu_2$ correlation observed in this source, but is inconsistent in detail. This is shown in Fig. 10. The top

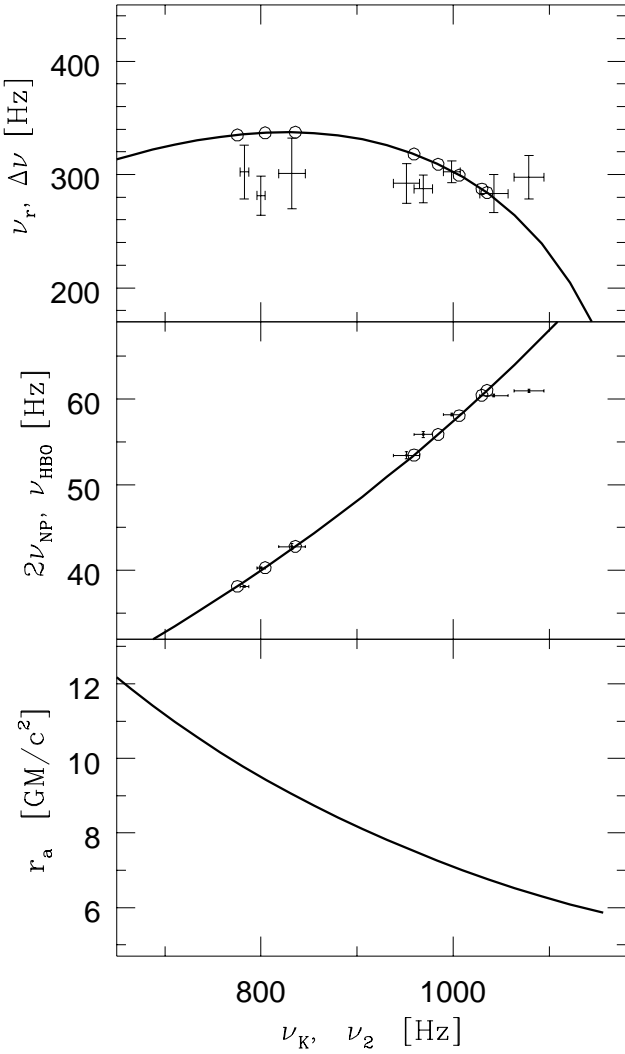


Figure 11. The geodesic sequence around UU stars that provides the best *simultaneous* fit to the ν_1 - ν_2 and ν_{HBO} - ν_K data for GX 17+2. The best-fit parameters are $M = 2.21 M_\odot$, $r_p = 5.0 M \approx 1.7 R_e$, and $\nu_s = 660$ Hz; $\chi^2/\text{dof} = 4.3$. The open circles show the frequency triplets $\{\nu_{\text{AP},i}, \nu_{K,i}, 2\nu_{\text{NP},i}\}$ that fit best. *Top panel:* Comparison of the resulting ν_r - ν_K relation with the observed $\Delta\nu$ - ν_2 correlation. *Middle panel:* Comparison of the resulting $2\nu_{\text{NP}}$ - ν_K relation with the observed ν_{HBO} - ν_2 correlation. *Bottom panel:* Circumferential apastron radii of the highly eccentric geodesics that give the frequencies plotted in the upper and middle panels.

panel compares the ν_r - ν_K relation given by the best-fitting sequence of HEGs with the observed $\Delta\nu$ - ν_2 correlation. Very highly eccentric geodesics ($r_a/r_p \approx 4$) are required in order to obtain an acceptable fit. The χ^2/dof is substantially less than 1 because of the large uncertainties reported for the ν_1 and ν_2 measurements. The fit is relatively insensitive to the spin frequency, for low to moderate spin frequencies.

The middle panel of Fig. 10 compares the $2\nu_{\text{NP}}$ - ν_K relation given by the sequence of HEGs used in the top panel that is most similar to the observed ν_{HBO} - ν_2 correlation. The relation shown is not a joint fit to the HBO and kilohertz QPO frequencies, but was instead obtained by adjusting the spin frequency to give the $2\nu_{\text{NP}}$ - ν_K relation that is closest to

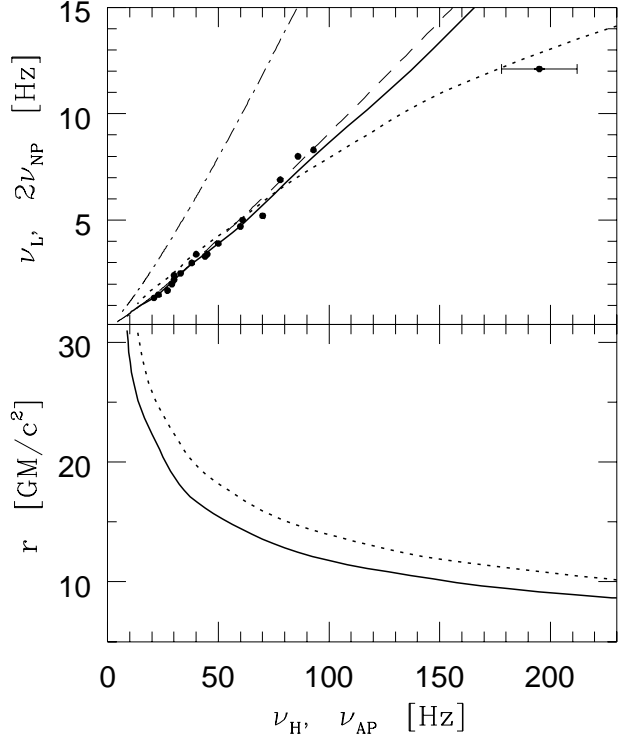


Figure 12. *Upper panel:* Comparison of the $2\nu_{\text{NP}}$ - ν_{AP} relations given by sequences of infinitesimally eccentric geodesics with the correlation between the frequencies ν_L and ν_h observed in Cir X-1. The solid and dotted curves show respectively the frequency relations given by sequences of MEGs around UU stars that give relations similar to the ν_L - ν_h correlation observed at $\nu_h < 100$ Hz, for $\nu_s = 700$ Hz ($M = 2.1 M_\odot$, $j = 0.26$) and $\nu_s = 900$ Hz ($M = 1.3 M_\odot$, $j = 0.50$). The dashed and dash-dotted curves show respectively the $2\nu_{\text{NP}}$ - ν_{AP} relations given by moderately eccentric geodesics around black holes with the same values of M and j as for the high- and low-mass neutron stars. *Lower panel:* Circumferential radii of the neutron star geodesics that give the frequencies plotted in the upper panel.

the observed ν_{HBO} - ν_2 correlation. The spin frequency that gives the best fit is 550 Hz. Although the $2\nu_{\text{NP}}$ - ν_K relation passes near the ν_{HBO} - ν_2 data, it misses many of the data points by much more than their uncertainties. The best-fitting ν_{AP} - ν_2 relation clearly does not correctly predict the ν_{HBO} - ν_2 correlation observed.

We then explored whether an acceptable *joint* fit to the ν_1 - ν_2 and ν_{HBO} - ν_2 correlations is possible. Fig. 11 shows the $2\nu_{\text{NP}}$ - ν_K and ν_{AP} - ν_2 relations given by the geodesic sequence that best fits both the ν_{HBO} - ν_2 and the ν_1 - ν_2 data. The high precision of the HBO frequency measurements forces the fit to make the $2\nu_{\text{NP}}$ values agree closely with them. However, this is possible only if the eccentricity of the geodesics is reduced, but this makes the ν_{AP} - ν_K relation steeper than the observed ν_1 - ν_2 correlation. The best-fit mass is driven to the maximum stable mass in an effort to compensate, but the compensation is insufficient to give an acceptable fit. Also, the periastron radius is driven far from the stellar surface ($r_p = 1.7 R_e$). Although the geodesics favoured by the attempt to fit jointly the ν_{HBO} - ν_2 and ν_1 - ν_2 data are less eccentric than those required by the ν_1 - ν_2 data, they are still highly eccentric ($r_a/r_p \approx 2$).

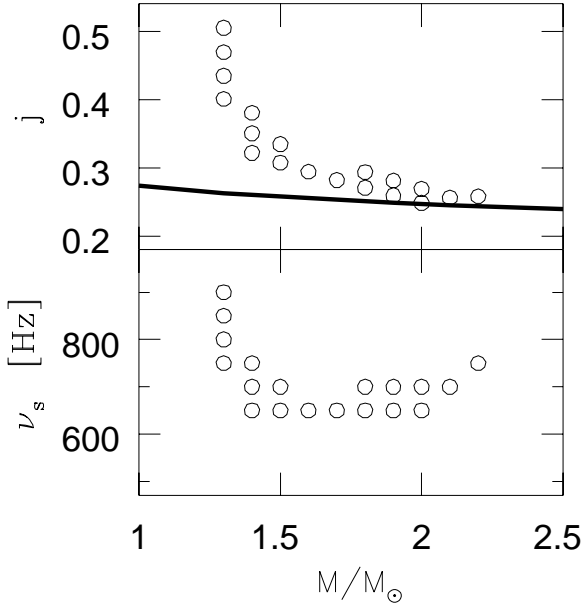


Figure 13. EOS UU-based neutron star models (open circles) that allow $2\nu_{\text{NP}}-\nu_{\text{AP}}$ relations similar to the $\nu_{\text{L}}-\nu_{\text{H}}$ correlation observed in Cir X-1 for $\nu_{\text{H}} < 100$ Hz. The solid line in the upper panel shows for comparison the j - M track along which sequences of geodesics around a spinning black hole can be constructed that give $2\nu_{\text{NP}}-\nu_{\text{AP}}$ relations similar to the observed $\nu_{\text{L}}-\nu_{\text{H}}$ correlation.

3.5 Cir X-1 QPO frequencies

Although the peculiar accreting X-ray star Cir X-1 is generally thought to be a neutron star (see Tennant, Fabian & Shafer 1986), Psaltis et al. (1999b) have suggested that its QPOs may be related to some of the QPOs observed in black-hole candidates, because power spectra of its X-ray emission are similar in some ways to the power spectra of black holes. SVM have proposed that the frequencies ν_{H} and ν_{L} of the higher- and lower-frequency features observed in Cir X-1 are the apsidal precession frequency ν_{AP} and twice the nodal precession frequency ν_{NP} of a sequence of slightly inclined IEGs around a neutron star, although they did not attempt a fit of the resulting frequency relations with the frequencies of the QPOs observed in Cir X-1.

Here we first investigate whether a sequence of IEGs can be found that gives a $2\nu_{\text{NP}}-\nu_{\text{AP}}$ relation that is consistent both with the QPO frequencies reported by Shirey et al. (1996, 1998) and Shirey (1998), and with the centroid frequencies of the peaked noise and QPO reported by Tennant (1987). No error bars were reported by Shirey et al., so our conclusions are necessarily tentative. The solid and dashed lines in Fig. 12 show the $2\nu_{\text{NP}}-\nu_{\text{AP}}$ relations given by the two sequences of IEGs that roughly bracket the range of masses and spin frequencies that agree qualitatively with the observed $\nu_{\text{L}}-\nu_{\text{H}}$ correlation for $\nu_{\text{H}} < 100$ Hz (see Fig. 13). In order to achieve qualitative agreement with the observed frequency correlation, the neutron star must be rapidly spinning ($\nu_s \gtrsim 650$ Hz) and the radii of the geodesics in the sequence must vary smoothly by a factor of 2.5, from $\sim 25 M$ to $\sim 10 M$, as the frequencies increase.

Inclusion of the higher-frequency ($\nu_{\text{L}} \approx 12$ Hz, $\nu_{\text{H}} \approx 200$ Hz) measurement reported by Tennant (1987) makes it much more difficult to find a sequence of geodesics that

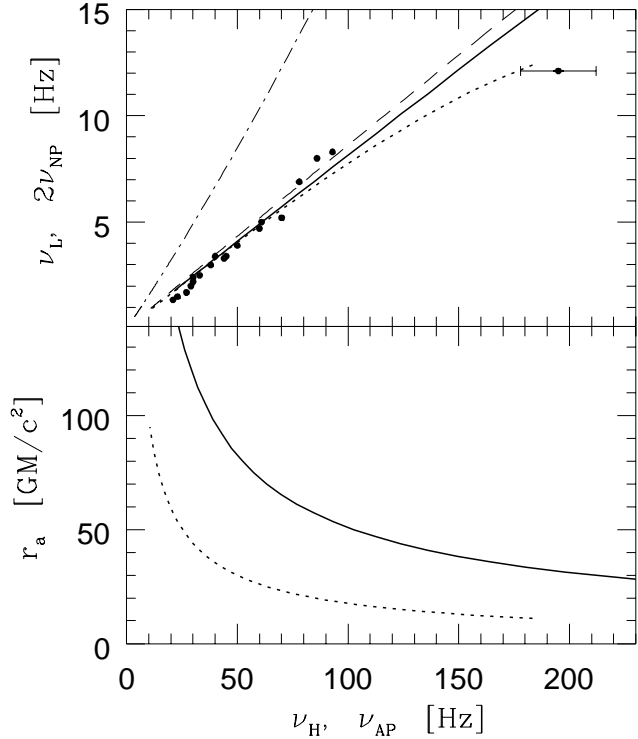


Figure 14. *Upper panel:* Comparison of the $2\nu_{\text{NP}}-\nu_{\text{AP}}$ relations given by sequences of highly eccentric geodesics with the correlation between the frequencies ν_{L} and ν_{H} observed in Cir X-1. The solid and dotted curves show respectively the frequency relations given by sequences of HEGs around UU stars that give relations similar to the $\nu_{\text{L}}-\nu_{\text{H}}$ correlation observed at $\nu_{\text{H}} < 100$ Hz, for $\nu_s = 550$ Hz ($M = 2.2 M_{\odot}$, $j = 0.18$, $r_p = 4.1 M$) and $\nu_s = 900$ Hz ($M = 1.3 M_{\odot}$, $j = 0.50$, $r_p = 11.0 M$). The dashed and dash-dotted curves show, for comparison, the $2\nu_{\text{NP}}-\nu_{\text{AP}}$ relations given by geodesics around black holes with the same values of M , j , and r_p as for the high- and low-mass neutron stars. *Lower panel:* Circumferential radii of the neutron star geodesics that give the frequencies plotted in the upper panel.

gives a frequency relation similar to the observed correlation. Only IEGs around stars with very low masses and very high spin rates give frequency relations that pass close to the lower-frequency data of Shirey et al. (1996, 1998) and then bend over sufficiently to pass near the higher-frequency measurement. Sufficient flattening of the $2\nu_{\text{NP}}-\nu_{\text{AP}}$ relation is achieved only for stars that are highly deformed by their rapid spins and therefore have large mass quadrupole moments whose effect largely cancels (at small radii) the prograde precession produced by frame-dragging. The effect of a large mass quadrupole may be seen clearly in Fig. 12 by comparing the $2\nu_{\text{NP}}-\nu_{\text{AP}}$ relations for neutron stars with the relations for black holes with the same M and j ; notice the particularly large difference for $M = 1.3 M_{\odot}$ and $j = 0.50$; the neutron star model is still fairly far from the mass-shedding limit, which is $0.93 M_{\odot}$.

Given the difficulty of approximating the $\nu_{\text{L}}-\nu_{\text{H}}$ correlation observed in Cir X-1 using IEG sequences, we explored whether it would be easier to reproduce the correlation using a sequence of HEGs. Our results are shown in Fig. 14. The lower-frequency portion of the $\nu_{\text{L}}-\nu_{\text{H}}$ correlation drives inclusion of very highly eccentric ($r_a/r_p > 6$) geodesics that extend far from the neutron star ($r_a/R_e > 10$) in the se-

Table 3. Fits of geodesic sequences to the measured frequencies of the kilohertz and lower-frequency QPOs.

Source	Model	EOS	ν_s [Hz]	$M[M_\odot]$	j	R_e [km]	R_e	r_{isco}	r_p	$r_{\text{a,min}}$	$r_{\text{a,max}}$	χ^2/dof	$n - p^a$	Fig.
Sco X-1	IEG	— ^b	0	1.99	0	10.7	3.64	6.0	r_a	6.2	7.0	38	72 – 37	1
	IEG	UU	450	2.21	0.145	9.8	3.02	5.52	r_a	5.7	6.5	35.5	72 – 37	1
	MEG ^c	— ^b	0	1.90	0	10.8	3.86	6.00	6.25	6.4	8.4	— ^c	— ^c	2
	MEG	UU	450	2.21	0.145	9.8	3.02	5.52	5.52	5.9	7.8	21	72 – 38	2
	MEG ^c	L	300	1.94	0.197	15.3	5.35	5.51	6.18	6.3	8.0	— ^c	— ^c	2
	MEG ^c	L	600	1.98	0.423	16.2	5.57	— ^d	6.17	6.3	7.8	— ^c	— ^c	2
	HEG	— ^b	0	1.89	0	10.8	3.88	6.00	5.3	8.9	11.0	1.4	72 – 38	3
	HEG	— ^b	0	1.86	0	10.0	3.65	6.00	5.1	9.8	11.8	2.2	72 – 38	3
	HEG	UU	450	2.13	0.158	10.5	3.32	5.49	4.9	8.0	10.0	1.4	72 – 38	9
	HEG	UU	500	2.16	0.173	10.4	3.27	5.44	4.8	8.0	10.0	1.4	72 – 38	9
	HEG	UU	550	2.18	0.187	10.2	3.19	5.40	4.8	7.8	9.8	1.4	72 – 38	9
GX 340+0	HEG	— ^b	0	1.86	0	10.0	3.66	6.00	5.8	10.6	16.2	2.3	12 – 8	4
	HEG	— ^b	0	2.12	0	10.3	3.30	6.00	7.0	7.0	11.1	0.8	12 – 8	4
4U 1728–34	IEG	UU	363	1.92	0.140	10.9	3.85	5.57	r_a	5.9	6.8	14.7	16 – 9	—
	IEG	UU	900	2.20	0.314	10.6	3.24	5.01	r_a	5.3	6.1	9.4	16 – 9	—
	HEG	UU	363	1.76	0.149	11.1	4.27	5.55	4.7	9.9	12.7	1.7	16 – 10	5,7
	HEG	AU δ	363	1.76	0.156	11.6	4.46	5.54	4.7	9.9	12.7	1.7	16 – 10	5
	HEG	L	363	1.97	0.239	15.4	5.30	5.44	5.3	6.2	8.7	8.6	16 – 10	5
GX 5–1	HEG	— ^b	0	2.17	0	10.1	3.16	6.00	6.5	6.5	13.5	3.6	20 – 12	6
	HEG	— ^b	0	2.09	0	10.4	3.38	6.00	6.5	6.5	13.9	1.2	18 – 11	6
	HEG	UU	100	2.20	0.032	9.8	3.02	5.89	6.3	6.7	13.5	3.6	20 – 12	8
	HEG	UU	363	2.21	0.117	9.8	3.02	5.62	5.8	7.0	14.9	4.5	20 – 12	8
	HEG	UU	600	2.22	0.194	9.9	3.02	5.37	5.3	7.6	16.0	5.6	20 – 12	8
GX 17+2	HEG	UU	550	1.81	0.224	11.1	4.16	5.35	4.2	12.4	16.0	0.39	16 – 10	10
	HEG+NP	UU	660	2.21	0.220	10.1	3.10	5.29	5.0	6.9	10.0	4.3	24 – 11	11
Cir X-1	NCG	UU	700	2.10	0.256	10.8	3.48	5.21	r_a	9	22	— ^e	— ^e	12
	NCG	UU	900	1.30	0.509	12.6	6.56	— ^d	r_a	11	26	— ^e	— ^e	12
	HEG	UU	550	2.20	0.184	10.2	3.13	5.40	4.1	34	150	— ^e	— ^e	14
	HEG	UU	900	1.30	0.509	12.6	6.56	— ^d	11	11	63	— ^e	— ^e	14

^aNumber of frequency measurements (n) minus the number of parameters in the model (p). ^bFits for nonrotating stars do not depend on the EOS, provided that it is hard enough to support the best-fit stellar mass and that $R_e < r_{p,\text{min}}$. The values of R_e listed for all nonrotating stars are for models constructed using the UU EOS, except for the $1.86 M_\odot$ stars, which were constructed using EOS C. ^cThese models are not fits and would give very large values of χ^2/dof . They are the geodesic sequences reported by SV as adequately fitting the Sco X-1 kilohertz QPO frequency data (see text). ^dNo innermost stable circular orbit exists, because the radius of the star is too large. ^eNo formal fits were possible, because no errors have been reported for most of the frequency measurements used; the fit was therefore done by eye, giving each point the same weight.

quence of HEGs. Inclusion of the higher-frequency measurement of Tenant (1987) again makes it much more difficult to find a sequence of geodesics that gives a frequency relation similar to the observed correlation. Only sequences of HEGs around stars with very low masses and very high spin rates give frequency relations that pass near all the measurements. The geodesic sequences that work best have infinitesimally or moderately eccentric geodesics as their most compact members, but even these geodesics have periastron radii much larger than the large equatorial radii of these stellar models ($r_p/R_e = 1.7$).

4 POWER DENSITY SPECTRA

SV, SVM, and Karas (1999) simply assumed that the most prominent frequencies in the X-ray waveforms produced by clumps moving on geodesics around a neutron star are $2\nu_{\text{NP}}$, ν_{AP} , and ν_{K} . No attempt was made to compute the frequencies that would be generated or the relative amplitudes of the

oscillations at these frequencies. Here we report calculations of the frequencies and amplitudes that would be produced.

In order to determine which are the dominant frequencies that would be generated and the relative amplitudes of the oscillations at these frequencies, we carried out an extensive suite of time-dependent, numerical simulations of the geodesic motion of clumps around spinning neutron stars. For the purposes of this investigation we simply assumed that all clumps are formed and move on the same geodesic, that they are held together by some force, and that they move forever on this same geodesic. We modeled the clumps as spheres of constant radius d . In order to facilitate the computations, we assumed $d = 0.1R_e$, which is about 100 times larger than allowed by the dynamical constraints (see Section 5). We treated the motion of the clumps in full general relativity and took into account special relativistic Doppler and other effects on the radiation absorbed and emitted by the clumps, but we did not perform ray tracing. Results using full ray tracing would be qualitatively similar to the results reported here. We surveyed a broad range of geodesic

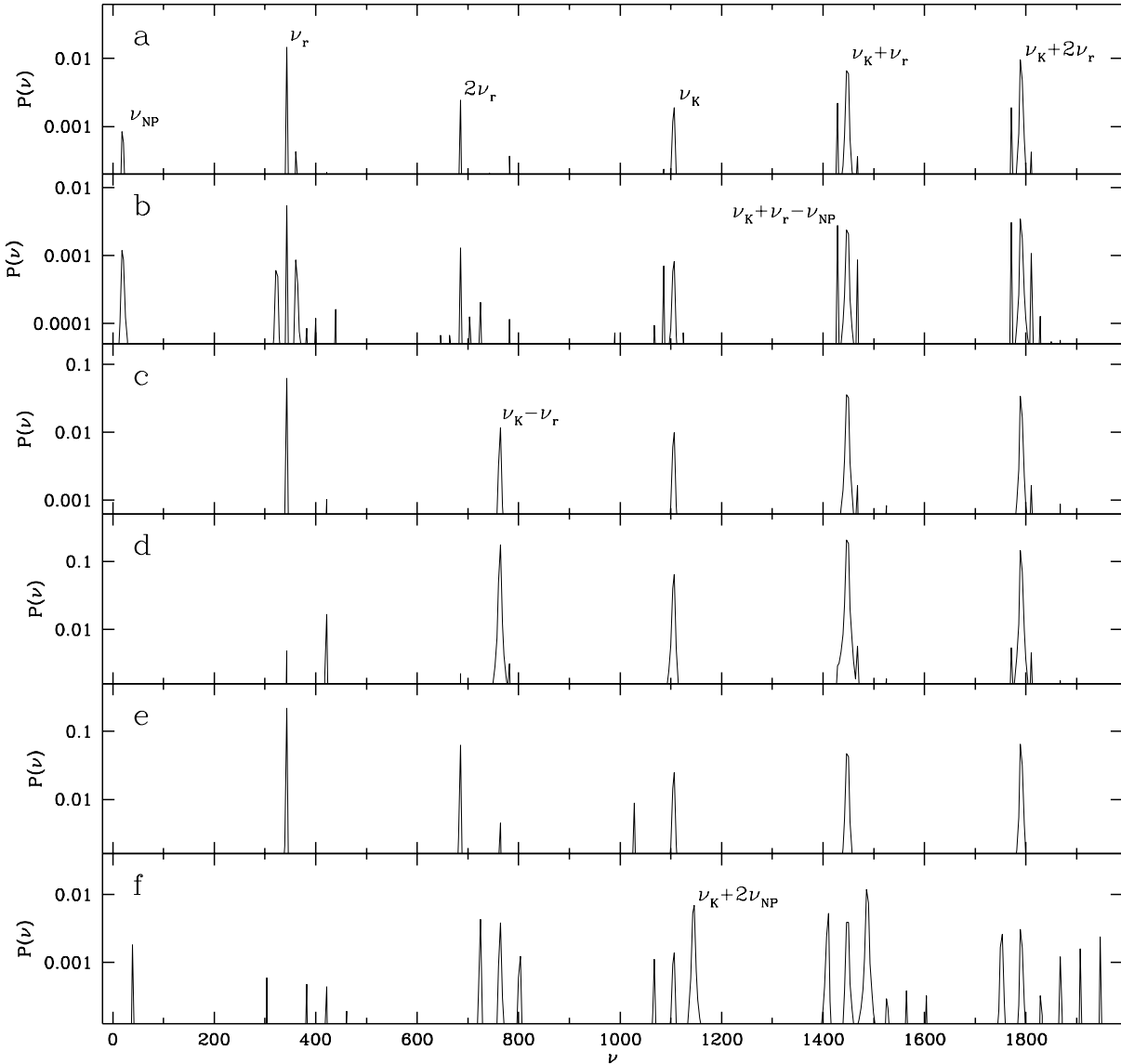


Figure 15. Typical power spectra produced by six different effects, for roughly spherical clumps on highly eccentric, tilted geodesics around a spinning neutron star. The heights of the peaks are not proportional to their total power, because their widths are different (total powers are listed in Table 4). From top to bottom, the effects considered are (see text for details): (a) occultation of a uniformly bright neutron star surface; (b) occultation of a belt with a Gaussian brightness distribution of semi-width $0.1R_e$ around the stellar equator; (c) reflection of radiation from a uniformly bright neutron star surface; (d) radiation by a clump with a radius-independent proper luminosity; (e) radiation by a clump with a radius-dependent proper luminosity; (f) radiation by a clump in a tilted orbit that emits only while it is passing through a rarified disc of height $h(r) = 0.05r$ in the equatorial plane of the system. In this example, $M = 1.76 M_\odot$, $\nu_s = 363$ Hz, $r_p = 4.7M$, and $r_a = 10.0M$, yielding $\nu_k = 1107$ Hz, $\nu_r = 343$ Hz, and $\nu_{NP} = 19$ Hz. The geodesic was assumed to be inclined 10° relative to the equatorial plane. The line of sight was assumed to be inclined 45° . As explained in the text, the actual power spectrum produced by a particular clump model is a linear combination of two or more of the spectra shown.

parameters, including r_p , r_a , and the tilt of the geodesic, and a wide range of viewing angles.

4.1 Highly eccentric geodesics

We simulated six different effects that could modulate the X-ray flux seen by a distant observer. The six panels of Fig. 15 show power spectra that are typical of the spectra produced by each of these effects, for clumps moving on geodesics with the high eccentricities required to produce kilohertz QPO frequencies qualitatively similar to those observed in

the atoll and Z sources. The heights of the peaks are not proportional to their total power, because the motions involved are not periodic, which causes the widths of the peaks to differ. The frequencies and relative total powers of the most prominent peaks are listed below in Table 4. As discussed further below, the actual power spectrum produced by a particular clump model is a linear combination of two or more of the spectra shown in Fig. 15. We now discuss briefly each of six effects (the labels a-f used here match the labels of the panels in Fig. 15).

(a) *Occultation of the stellar surface.* An optically thick

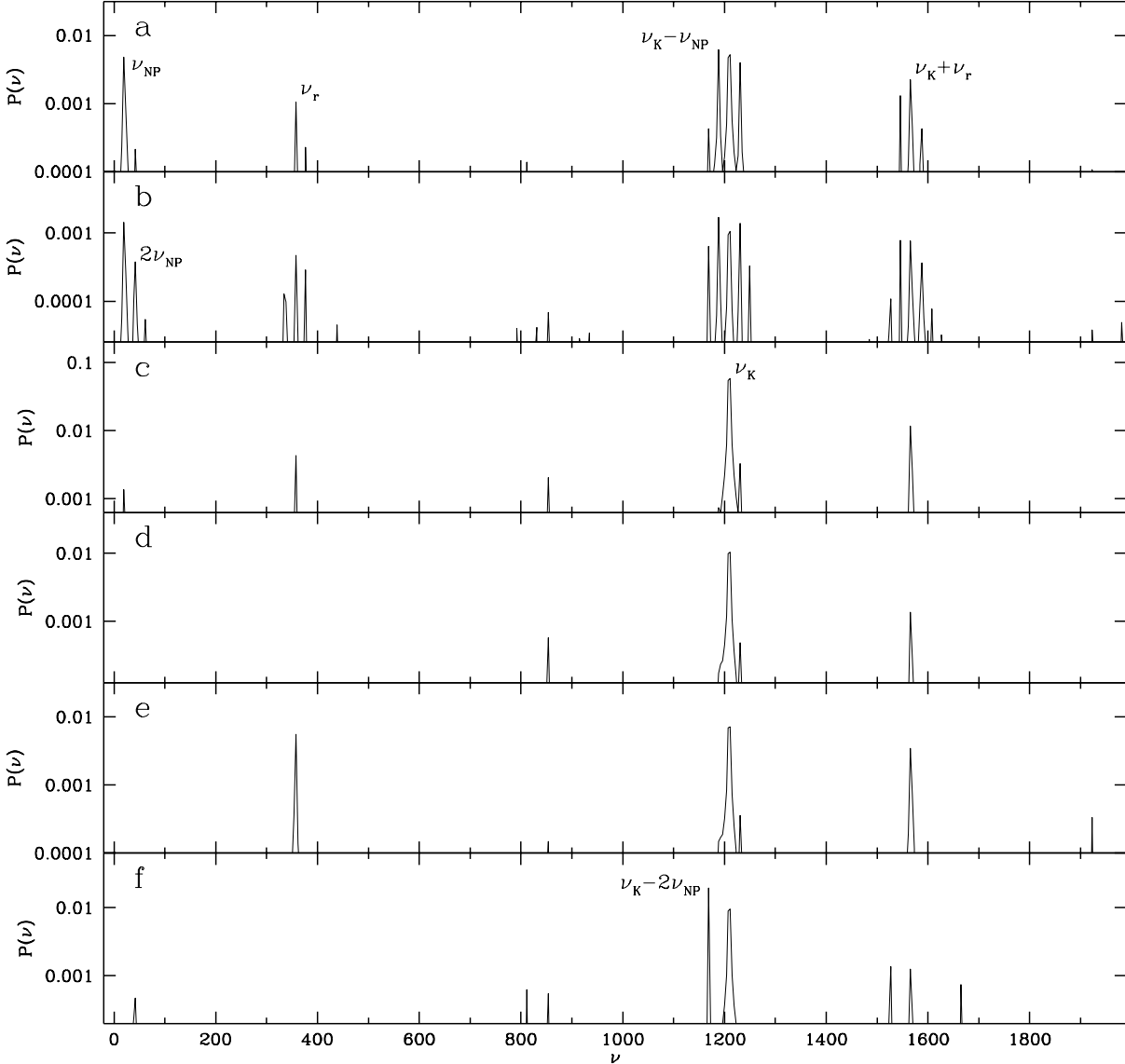


Figure 16. Typical power spectra produced by the same six effects considered in Fig. 15, but for moderately eccentric geodesics. As in Fig. 15, the heights of the peaks are not proportional to their total power, because their widths are different (total powers are listed below, in Table 4). The stellar mass and spin rate and the inclinations of the geodesic and line of sight are the same as in Fig. 15, but $r_p = 5.6M$ and $r_a = 6.7M$, corresponding to an eccentricity $\varepsilon = 0.09$ and yielding $\nu_K = 1211$ Hz, $\nu_r = 358$ Hz, and $\nu_{NP} = 19$ Hz. As explained in the text, the actual power spectrum produced by a particular clump model is a linear combination of two or more of the spectra shown.

clump moving around a neutron star on a geodesic may occult a portion of the stellar surface, thereby modulating the X-ray flux from the surface seen by a distant observer. Occultation occurs only for geodesics that satisfy $r_p < (R_e + d)/\cos i$, i.e., that closely approach the stellar surface. Some of the best-fit geodesics listed in Table 3 do not satisfy this constraint unless the observer's sightline is close to the plane of the disc.

In the absence of apsidal and nodal precession, the star would be occulted periodically, with frequency $\nu_K = \nu_r$. However, general relativistic effects near the neutron star make $\nu_K > \nu_r$. For the geodesics considered here, a clump typically orbits the star three or four times each time it moves radially inward and outward at the radial epicyclic

frequency ν_r . The rate of azimuthal phase advance varies significantly with the radial position of a clump and hence the occultation caused by the azimuthal motion is not periodic. The only strictly periodic motion is the radial epicyclic motion, which causes the observed flux to vary with frequency ν_r as the extent of the occultation increases and decreases with the motion of the clump toward and away from the star (depending on the value of r_a and the inclination of the geodesic and the line of sight, a clump that is near r_a may not occult the star at all).

The strongest peaks in the power density spectrum of the X-ray waveform are at the radial epicyclic frequency ν_r and the combination frequencies $\nu_K + \nu_r$ and $\nu_K + 2\nu_r$ (see Fig. 15a). The next strongest peak is at $2\nu_r$. Weaker nodal

precession sidebands appear at $\nu_K + \nu_r - \nu_{NP}$ and $\nu_K + 2\nu_r - \nu_{NP}$ in this power spectrum and the others discussed below only if the geodesic is significantly tilted. *There is much less power at the azimuthal frequency ν_K and almost none at the apsidal precession frequency $\nu_{AP} = \nu_K - \nu_r$.* These are the frequencies that SV, SVM, and Karas (1999) assumed would be the dominant frequencies in the power spectrum. The power in the peak at ν_K is typically ~ 4 –5 times less than the power in the peak at ν_r ; the power at ν_{AP} is too low for the peak to be visible in Fig. 15a. Nodal precession modulates the angle between the orbital plane and the observer's line of sight, producing a very weak peak at ν_{NP} ; there is no significant power at $2\nu_{NP}$.

(b) *Occultation of a bright equatorial band.* If radiation comes predominantly from a narrow belt around the star's rotation equator, nodal precession has a stronger effect on the waveform. Fig. 15b shows a typical power spectrum of the waveform for this situation. In this example, the surface brightness of the star was assumed to vary as $\exp(-z^2/\sigma^2)$, where z is the distance of the point on the stellar surface from the equatorial plane and $\sigma = 0.1R_e$.

The strongest peaks are again at ν_r , $\nu_K + \nu_r$, and $\nu_K + 2\nu_r$. The next strongest peaks, which are about half as strong, are at $\nu_K + \nu_r - \nu_{NP}$ and $\nu_K + 2\nu_r - \nu_{NP}$. There is a peak at ν_{NP} that is slightly weaker than these nodal-precession sidebands. *Again, there is much less power at ν_K and almost none at ν_{AP} .* The peak at ν_K is ~ 3 –4 times weaker than the three strongest peaks in the power spectrum and is significantly weaker even than the peak at ν_{NP} . The next strongest peaks, which have almost as much power as the peak at ν_K , are at the nodal sideband frequencies $\nu_r - \nu_{NP}$, $\nu_r + \nu_{NP}$, and $\nu_K + 2\nu_r + \nu_{NP}$. The peak at ν_{AP} is too weak to be visible and there is no significant power at $2\nu_{NP}$.

(c) *Reflection of stellar radiation by clumps.* Fig. 15c shows the power spectrum for a typical waveform generated by clumps that reflect radiation coming from the stellar surface. In this example, we assumed that the surface brightness of a clump varies with its distance r from the center of the star as $1/r^2$ and that the flux is proportional to its surface brightness and the projected area of the illuminated part of the surface seen by the distant observer. The Doppler shifts caused by the velocity of the clump relative to the stellar surface and to the observer were included.

The strongest peak produced by reflection is at $\nu_K + \nu_r$. There are also strong peaks at ν_r and $\nu_K + 2\nu_r$. There are peaks at ν_K and ν_{AP} , but the power in these peaks is ~ 4 –5 times less than in the peak at $\nu_K + \nu_r$ and ~ 3 –4 times less than in the peaks at ν_r and $\nu_K + 2\nu_r$. There is no significant power at either ν_{NP} or $2\nu_{NP}$.

(d) *Radiation by constant temperature clumps.* Significant radiation by clumps with the small size and high density required by gas dynamical constraints (see Section 5) is ruled out by their very small areas compared to that of the accreting star and by the upper bound on their temperature imposed by their origin in a cool disc flow and the requirement that they be in pressure equilibrium with their environment (otherwise they will expand and dissipate on a timescale much shorter than the lower bound on the durations of their wavetrains imposed by the observed coherence of the kilohertz QPOs). Nevertheless, for completeness we explored the waveform that would be produced by such radiation.

Even if the luminosity of a clump is constant in time in its rest frame, the general relativistic redshift and other effects will cause the luminosity seen by a distant observer to increase and decrease with the clump's distance r from the center of the star, which varies at the radial epicyclic frequency. For the illustrative calculations reported here, we took into account only the Doppler shift caused by the clump's motion relative to the distant observer.

A typical power spectrum is shown in Fig. 15d. The strongest peak is at $\nu_K + \nu_r$. There is also a peak at $\nu_K + 2\nu_r$ which is about half as strong. There is a peak at ν_{AP} , which is also about half as strong as the peak at $\nu_K + \nu_r$, as well as a peak at ν_K , which is ~ 4 times weaker than the peak at $\nu_K + \nu_r$ and only about half as strong as the peak at $\nu_K + 2\nu_r$. There are no other significant peaks. Hence, *even in this case the peaks at $\nu_K + \nu_r$ and $\nu_K + 2\nu_r$ are as strong or stronger than the peaks at ν_K and ν_{AP} .*

(e) *Radiation by clumps heated by radiation from or interaction with the star.* Again, significant radiation by clumps is ruled out by their very small areas and by the upper bound on their temperature imposed by the requirement that they be in pressure equilibrium. Furthermore, any interaction of the clumps with the stellar surface or with a stellar magnetic field that is strong enough to release an appreciable fraction of their kinetic energy would disrupt them and cause their orbits to decay. Nevertheless, for completeness we also explored the waveform that would be produced by such radiation.

The rest-frame luminosity of a clump heated by radiation from the star or by interaction with a stellar atmosphere or magnetic field necessarily varies strongly with r . The luminosity seen by a distant observer is also affected by the variation of the Doppler shift with r . For the illustrative calculations reported here, we assumed that heating causes the brightness of a clump to vary with radius as $1/[(r - R_e)^2 + 0.01R_e^2]$.

A typical power spectrum is shown in Fig. 15e. The strongest peak is at ν_r , with peaks at $\nu_K + \nu_r$ and $\nu_K + 2\nu_r$ that are about half as strong and a peak at $2\nu_r$ that is about a third as strong. *There is a peak at ν_K , but it is ~ 5 times weaker than the main peak and less than half as strong as the peaks at $\nu_K + \nu_r$ and $\nu_K + 2\nu_r$; there is no significant power at ν_{AP} , ν_{NP} , or $2\nu_{NP}$.*

(f) *Interaction of clumps with a rarefied gaseous disc.* Finally, we consider the possibility that the luminosity increases when clumps on tilted geodesics pass through the equatorial plane. Such flaring could be caused, for example, by interaction of the clumps with a rarified, remnant gaseous disc in the plane near the star. The additional luminosity produced by enhanced dissipation would have to be very small in order to avoid causing the clumps' orbital motion to decay more rapidly than is allowed by the observed coherence of the kilohertz QPOs. This scenario was constructed specifically to produce a peak as strong as possible at $2\nu_{NP}$. The results presented here assume the clump brightness varies as $\exp(-z^2/h^2)$, where $h(r) = 0.05r$ is the height of the disc, but they are insensitive to the precise value of h .

Even in this scenario, the two strongest peaks are at $\nu_K + \nu_r + 2\nu_{NP}$ and $\nu_K + 2\nu_{NP}$. The next strongest peaks are at $\nu_K + \nu_r$ and $\nu_K + \nu_r - 2\nu_{NP}$ and have ~ 2.5 times less power than the peak at $\nu_K + \nu_r + 2\nu_{NP}$. There are two peaks

Table 4. Total power in the prominent peaks in the twelve typical power spectra shown in Figs. 15 and 16.¹

Frequency ²	HEG ($r_p = 4.7, r_a = 10.0$) ³						MEG ($r_p = 5.6, r_a = 6.7$) ³					
	a	b	c	d	e	f	a	b	c	d	e	f
ν_{NP}	0.10	0.40	—	—	—	—	0.54	0.82	—	—	—	—
$2\nu_{NP}$	—	—	—	—	—	—	—	0.24	—	—	—	—
ν_r	0.90	0.90	0.79	—	1	—	0.10	0.24	—	—	0.37	—
$\nu_r - \nu_{NP}$	—	0.21	—	—	—	—	—	0.12	—	—	—	—
$\nu_r + \nu_{NP}$	—	0.23	—	—	—	—	—	0.14	—	—	—	—
$2\nu_r$	0.16	0.22	—	—	0.30	—	—	—	—	—	—	—
$\nu_K - \nu_r$	—	—	0.21	0.54	—	0.23	—	—	—	—	—	—
$\nu_K - \nu_r - 2\nu_{NP}$	—	—	—	—	—	0.21	—	—	—	—	—	—
ν_K	0.22	0.27	0.24	0.26	0.21	0.12	1	1	1	1	1	1
$\nu_K - \nu_{NP}$	—	0.12	—	—	—	—	0.63	0.85	—	—	—	—
$\nu_K + \nu_{NP}$	—	—	—	—	—	—	0.40	0.68	—	—	—	—
$\nu_K - 2\nu_{NP}$	—	—	—	—	—	—	—	0.30	—	—	—	0.88
$\nu_K + 2\nu_{NP}$	—	—	—	—	—	0.63	—	0.17	—	—	—	—
$\nu_K + \nu_r$	0.89	0.86	1	1	0.47	0.40	0.26	0.45	0.12	—	0.27	—
$\nu_K + \nu_r - \nu_{NP}$	0.14	0.46	—	—	—	—	0.12	0.36	—	—	—	—
$\nu_K + \nu_r + \nu_{NP}$	—	0.15	—	—	—	—	—	0.25	—	—	—	—
$\nu_K + \nu_r - 2\nu_{NP}$	—	—	—	—	—	0.39	—	—	—	—	—	—
$\nu_K + \nu_r + 2\nu_{NP}$	—	—	—	—	—	1	—	—	—	—	—	—
$\nu_K + 2\nu_r$	1	1	0.72	0.53	0.50	0.24	—	—	—	—	—	—
$\nu_K + 2\nu_r - \nu_{NP}$	0.12	0.51	—	—	—	—	—	—	—	—	—	—
$\nu_K + 2\nu_r + \nu_{NP}$	—	0.19	—	—	—	—	—	—	—	—	—	—
$\nu_K + 2\nu_r - 2\nu_{NP}$	—	—	—	—	—	0.22	—	—	—	—	—	—

¹The total power in each peak is normalised to the total power in the strongest peak produced by each effect. ²Only peaks with total power $\geq 10\%$ of the strongest peak at frequencies $\leq 2,000$ Hz are listed. ³The six columns for the HEG and MEG models list the power ratios for the prominent frequencies produced by the six different effects discussed in the text. These are (a) occultation of a uniformly bright neutron star surface; (b) occultation of a belt with a Gaussian brightness distribution of semi-width $0.1R_e$ around the stellar equator; (c) reflection of radiation from a uniformly bright neutron star surface; (d) radiation by a clump with a radius-independent proper luminosity; (e) radiation by a clump with a radius-dependent proper luminosity; (f) radiation by a clump in a tilted orbit that emits only while it is passing through a rarified disc of height $h(r) = 0.05r$ in the equatorial plane of the system.

The actual power spectrum produced by a particular clump model is a linear combination of two or more of the spectra shown in Fig. 15. For example, a clump that reflects radiation from the stellar surface [effect (c)] or produces a flare of emission as it passes through the orbital plane [effect (f)] will generally also occult the star [effects (a) and (b)].

at ν_{AP} and $\nu_{AP} - 2\nu_{NP}$, but they have $\sim 4\text{--}5$ times less power than the peak at $\nu_K + \nu_r + 2\nu_{NP}$ and are no stronger than the peaks at $\nu_K + \nu_r$ and $\nu_K + \nu_r - 2\nu_{NP}$. There is also a peak at ν_K , but it has ten times less power than the peak at $\nu_K + \nu_r + 2\nu_{NP}$. The peak at $2\nu_{NP}$ has 12 times less power than the peak at $\nu_K + \nu_r + 2\nu_{NP}$ and 6 times less power than the peak at $\nu_K + 2\nu_{NP}$ (it is too weak to be listed in Table 4). There is no significant power at ν_{NP} .

We emphasise that *the actual power spectrum produced by a particular clump model is a linear combination of two or more of the spectra shown in Fig. 15*. For example, a clump that reflects radiation from the stellar surface [effect (c)] or produces a flare of emission as it passes through the orbital plane [effect (f)] will generally also occult the star [effects (a) and (b)]; indeed, occultation is typically the dominant effect.

4.2 Nearly circular geodesics

For completeness, we also computed the waveforms that would be produced by each of the six effects just discussed if the clumps were moving on nearly circular geodesics, even though such geodesics are excluded by the observed QPO frequency relations. Fig. 16 shows power spectra of the typical waveforms produced by such geodesics. The frequencies and relative total powers of the most prominent peaks are again listed in Table 4.

For orbits with eccentricities $\varepsilon \equiv (r_a - r_p)/(r_a + r_p) \lesssim 0.1$, there is (almost) always a strong peak at ν_K . Usually, there is also a significant peak at $\nu_K + \nu_r$. Occultation can produce relatively strong peaks at ν_{NP} and $2\nu_{NP}$ and significant peaks at the nodal sideband frequencies of ν_K and $\nu_K + \nu_r$, but most effects do not produce peaks at these frequencies.

We emphasise that for infinitesimally or only moderately eccentric orbits, r must be $< (R_e + d)/\cos i$ for the

star to be even partially occulted. Hence, in order to produce any occultation, such geodesics must have azimuthal frequencies

$$\nu_K > 1550 \text{ Hz} (\sqrt{2} \cos i)^{3/2} \left(\frac{10 \text{ km}}{R_e + d} \right)^{3/2} \left(\frac{M}{2M_\odot} \right)^{1/2}. \quad (3)$$

This requirement is inconsistent with the interpretation of the upper kilohertz QPO frequency as an azimuthal frequency, unless all the kilohertz QPO systems are highly inclined, which is unlikely and contradicts other evidence concerning their inclinations.

5 GAS DYNAMICAL CONSTRAINTS

The geodesic precession model assumes that at a particular radius the accretion flow onto the neutron star changes from a disc flow to gas clumps moving on geodesics with the same or very similar apastron and periastron radii r_a and periastron r_p . It assumes further that the geodesics that are populated by clumps at any given time have the azimuthal, apsidal precession, and nodal precession frequencies required to explain the frequencies of the QPOs observed in the atoll and Z sources. Finally, the hypothesis assumes that as the accretion rate varies, the orbital parameters of the geodesics that are populated change in the way needed to produce the observed correlated variation of ν_L or ν_{HBO} , ν_1 , and ν_2 .

As we now discuss, the behaviour of the accreting gas required by the geodesic precession hypothesis is very difficult to achieve in any physically consistent gas dynamical picture. For the purposes of the present section we set aside the results of the previous section, which showed that the frequencies generated by orbiting clumps are not the frequencies assumed by previous workers, and focus on the gas dynamical requirements of the model.

5.1 Circularity of the flow in the disc

We begin by showing that the stream lines in the accretion disc are necessarily nearly circular, in contrast to the highly eccentric geodesics required to produce orbital frequencies qualitatively similar to the observed frequencies of the kilohertz QPOs. The reason is that the apsidal precession rate varies rapidly with the radius of the geodesic. Hence any eccentric, adjacent streamlines would intersect in less than an orbital period, creating strong shear stresses, pressure gradients, and possibly shock waves that will quickly circularise the motion.

To see this, consider gas streaming along two nearby, eccentric geodesics with periastron radii r_{p1} and $r_{p2} = r_{p1} + \delta r_p$. For the present purpose we assume the geodesics are ellipses in Euclidean space and describe each of them using the familiar radius-angle relation $r = r_p(1 + \varepsilon)/(1 + \varepsilon \cos \phi)$, where the angle ϕ is measured from the geodesic's periastron. Suppose the geodesics are initially concentric and aligned and have the same, finite eccentricity ε . In the absence of shear or pressure stresses, the different precession rates of the two geodesics will bring them into contact at the 'osculation' point after a time δt . The angle between the axes of the two ellipses at this time can be obtained from the osculation point conditions $r_1 = r_2$ and $[dr/d\phi]_1 = [dr/d\phi]_2$,

where the subscripts indicate the radius-angle relations for the two ellipses.

Solving for $\delta\phi$ gives, to the lowest order in $\delta r_p/r_p$, $\sin \delta\phi = (\delta r_p/r_p)(1 - \varepsilon^2)^{1/2}/\varepsilon$. The differential rate of periastron advance is $\delta\nu_{\text{AP}} \approx (\partial\nu_{\text{AP}}/\partial r_p)\delta r_p$. Using the lowest-order post-Newtonian expression for ν_{AP} (see Markovic 2000) we obtain

$$\delta t = \frac{(\delta\phi/2\pi)}{(\partial\nu_{\text{AP}}/\partial r_p)\delta r_p} \simeq \frac{1}{15\pi} \frac{(1 + \varepsilon)^{3/2}(1 - \varepsilon)^{1/2}}{\varepsilon} \frac{1}{\nu_{K,N}}, \quad (4)$$

where $\nu_{K,N} \equiv (1 - \varepsilon)^{3/2}(GM/r_p^3)^{1/2}/2\pi$ is the Newtonian Kepler frequency. Equation (4) shows that the two streamlines will intersect in less than one orbital period even if they are only very slightly eccentric ($\varepsilon \gtrsim 0.02$). Moderately or highly eccentric streamlines will intersect in much less than one orbital period.

In reality, the two streamlines will not cross. Instead, shear stresses and gas pressure forces will grow to oppose their differential apsidal precession, forcing the two streamlines to deviate from purely geodesic motion. The result will be to circularise both streamlines within a time $\sim \delta t$, i.e., in less than one orbital period.

5.2 Effects of tidal forces

The high coherence ($Q \sim 100$) of the kilohertz QPOs requires that the postulated gas clumps survive for at least Q orbital periods. However, the strong gravitational tidal force near the star will tidally disrupt clumps unless they are either confined by external forces or are very small.

The rapid damping of noncircular flow in the inner disc makes persistence of the highly eccentric geodesic motion required by the geodesic precession model impossible unless the clumps are isolated from the general gas flow, i.e., unless there is an extensive region around the star where the density of the interclump gas is negligible. The clumps therefore cannot be confined by the surrounding gas. Nor can they be confined by the stellar magnetic field, because the torque produced by a field strong enough to confine the gas in the clumps would be strong enough to cause them to deviate from purely geodesic motion. Therefore, the clumps can persist for Q orbital periods only if they are very small.

To estimate how long a clump of radius d can persist, consider two elements of the clump moving on concentric orbits with the same eccentricity and orientation but slightly different periastra r_p and $r_p + 2d$. Neglecting apsidal precession and other relativistic effects, the difference between the azimuthal frequencies of the two elements is $\delta\nu_{K,N} \approx (2d/r_p)(3/2)\nu_{K,N}$. Hence, after a time t the clump will be sheared out a distance $\Delta d \approx r_p 2\pi \delta\nu_{K,N} t$. The X-ray modulation produced by such a clump will certainly be markedly changed by the time the clump has been spread a quarter of the way around the star (i.e., over a phase interval of $\pi/2$). This will happen in less than Q orbital periods unless

$$\frac{d}{r_p} \ll \frac{1}{12Q} \approx 8 \times 10^{-4} \left(\frac{100}{Q} \right). \quad (5)$$

In the last expression on the right we have scaled Q by 100, the minimum value required for consistency with the observed coherence of the kilohertz QPOs. Inequality (5) is a

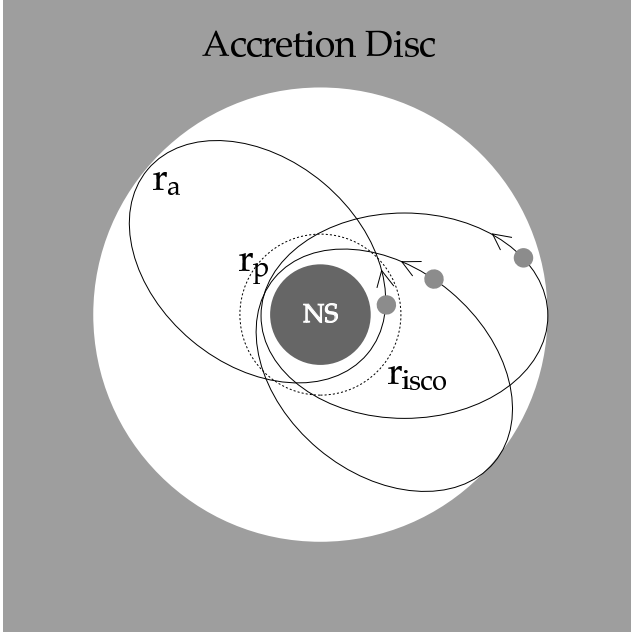


Figure 17. Schematic depiction of the breakup of the accretion disc into dense clumps on nearly identical highly eccentric geodesics as required by the geodesic precession model. Here r_a and r_p are the apastron and periastron radii of the geodesic, r_{isco} is the radius of the innermost stable circular orbit, and the dark disc shows the size of a typical neutron star. In reality, geodesics near the star are very open rosettes rather than ellipses: a clump on these geodesics would go around the star 3–4 times as it moves from r_a to r_p . The figure shows that the clumps have relative velocities comparable to their azimuthal velocities, even if they are on geodesics with similar values of r_a and r_p .

strong upper bound on the size of a roughly spherical clump that would survive tidal disruption for Q orbital periods. As we show below, this bound is a very significant constraint on precessing clump models.

5.3 Constraints on the gas density in the clumps

The requirement that the interaction of clumps with the interclump gas not affect significantly their orbits for Q orbital periods leads to a lower bound on the density ρ_c of the gas in the clumps relative to the density ρ_i of the interclump medium. As shown above, the interclump gas must follow nearly circular orbits; hence any clumps on highly eccentric geodesics must move at supersonic speeds through the interclump gas. Assuming that it can be held together by some means, a gas clump of size d moving with supersonic velocity $\mathbf{v}_c - \mathbf{v}_g$ through interclump gas of density ρ_i will experience a drag force

$$F_D = C_D d^2 \rho_i (\mathbf{v}_c - \mathbf{v}_g)^2 \sim C_D d^2 \rho_i v_c^2, \quad (6)$$

where C_D (~ 1) is the ballistic coefficient. A clump of mean density ρ_c has momentum $d^3 \rho_c v_c$ and hence persistence of geodesic motion for Q orbital periods would require a density ratio

$$\frac{\rho_c}{\rho_i} \gg \frac{r Q C_D}{d} \gg 10^5 C_D \left(\frac{Q}{100} \right)^2, \quad (7)$$

where in writing the last inequality on the right we have used condition (5).

The requirement that the clumps not collide too frequently leads to an even more stringent lower bound on the density of the gas in the clumps relative to the mean density near the star. The mean clump-clump collision rate near the star is $R = n_c \sigma v_{\text{rel}} \approx n_c 4\pi d^2 v_{\text{rel}}$, where n_c is the density of clumps near the star and v_{rel} is their typical relative velocity. Even if the clumps all move on geodesics with the same values of r_p and r_a , their periastron phases will be different (see Fig. 17) and hence they will approach each other with relative velocities that are comparable to v_K . Now $n_c = 3\bar{\rho}_c / (4\pi \rho_c d^3)$, where $\bar{\rho}_c$ is the mean mass density in the clumped region. Hence $R \approx 3(\bar{\rho}_c / \rho_c)(v_K / d)$. The observed coherence of the kilohertz QPOs requires $2\pi Q R r_p / v_K \lesssim 1$, or

$$\frac{\rho_c}{\bar{\rho}_c} \gtrsim \frac{6\pi r_p Q}{d} \gg 2 \times 10^6 \left(\frac{Q}{100} \right)^2, \quad (8)$$

where in the last inequality we have again used condition (5).

These dynamical constraints show that the density contrast in the clumps required by the geodesic precession hypothesis is enormously greater than the density contrasts and magnetic field fluctuations considered in the magnetospheric (Alpar & Shaham 1985; Lamb et al. 1985) and sonic-point (Miller et al. 1998) beat-frequency models of QPOs; in the latter models, the fluctuations have relative amplitudes $\lesssim 1$ and move with the mean flow. How clumps with such extremely high densities would form or persist in a gas dynamical flow and how they would be replenished are unknown. A large number of clumps would have to be produced to carry a substantial fraction of the accretion flow and produce significant X-ray modulation. Clumps would have to be formed from the gas in the region where the orbits are nearly circular and then “shot” quickly into the required highly eccentric orbits in an inner, highly rarefied region near the star, in order to avoid interaction with the gas moving on nearly circular orbits. However, any forces capable of producing the required sudden deviation from circular motion would also be strong enough to disrupt the clumps and cause them to deviate strongly from purely geodesic motion. As noted earlier, what picks out the particular geodesics required by the geodesic precession hypothesis is also unknown.

5.4 Implications for QPO amplitudes

The small size necessary for clumps to persist as long as required by the observed coherence of the kilohertz QPOs means that the projected area of a clump is only a very small fraction of the projected area of the stellar surface. The fractional area of a clump is

$$f = \frac{\pi d^2}{\pi R_p^2} < \frac{d^2}{r_p^2} \ll 7 \times 10^{-7}. \quad (9)$$

This is also an upper bound on the fractional modulation of the X-ray flux that can be produced by clumps, whether the modulation is caused by occultation of the surface of the star, reflection of radiation from the star, or emission from a clump at about the same temperature as the stellar surface.

6 DISCUSSION AND CONCLUSIONS

If it could be established that the frequencies of the most prominent humps, bumps, and QPOs observed in power spectra of the X-ray emission from neutron star and black hole LMXBs are simply the characteristic frequencies of gas clumps orbiting these objects and that hydrodynamic, radiation, and magnetic forces have no significant effects, so that their motion is purely geodesic motion, this would be an extraordinarily important result. In particular, it would mean that measurements of these frequencies would provide a very simple way to explore the effects of strong-field gravity and the properties of compact objects. This is why we have carefully investigated this suggestion. Here we discuss our principal results and summarize our conclusions.

6.1 Geodesics and frequency relations

We first explored whether sequences of geodesics could be found with azimuthal and apsidal precession frequencies ν_{AP} and ν_{K} that agree, respectively, with the observed frequencies ν_1 and ν_2 of the lower and upper kilohertz QPOs. We also investigated whether geodesic sequences could be found for which the first overtone $2\nu_{\text{NP}}$ of the nodal precession frequency and ν_{K} and ν_{AP} agree, simultaneously, with the frequencies of the low-frequency and kilohertz QPOs. Here we briefly summarise the results of these investigations.

6.1.1 Infinitesimally and moderately eccentric geodesics

In Section 3.1 we explored whether it is possible to construct sequences of infinitesimally or moderately eccentric geodesics that give $\nu_{\text{AP}}\text{-}\nu_{\text{K}}$ relations consistent with the observed correlations between ν_1 and ν_2 .

We first investigated infinitesimally eccentric geodesics. The geodesic precession hypothesis makes no predictions about the apastron and periastron radii r_{a} and r_{p} of the geodesics or how they vary, except that they must (obviously) be larger than the equatorial radius of the star. In exploring infinitesimally eccentric geodesics, we set $r_{\text{p}} = r_{\text{a}}$ and treated r_{a} as a free parameter, subject only to the requirement that it exceed the radius of the innermost stable circular orbit r_{isco} . The parameters in this model are therefore the EOS, mass, and spin frequency of the star, and an orbital radius for each pair of kilohertz QPO frequencies that was fit.

We found that the $\nu_{\text{AP}}\text{-}\nu_{\text{K}}$ relations given by the best-fitting sequences of infinitesimally eccentric geodesics are much steeper than the observed $\Delta\nu \equiv \nu_2 - \nu_1$ vs. ν_2 correlation. Our $\nu_{\text{AP}}\text{-}\nu_{\text{K}}$ relations are consistent with the $\nu_{\text{AP}}\text{-}\nu_{\text{K}}$ relations reported by SV, which are also much steeper than the frequency data presented in their paper. The qualitative disagreement between the best-fitting frequency relations for infinitesimally eccentric geodesics and the kilohertz QPO frequency data is indicated by the very large values of χ^2/dof found ($\gtrsim 35$ for the Z source Sco X-1 and $\gtrsim 10$ for the atoll source 4U 1728-34).

We note that the qualitative disagreement between the frequency relations for infinitesimally eccentric geodesics and the frequency data is a serious difficulty for the resonant ring model recently proposed by Psaltis & Norman (2000) to explain the QPOs in both neutron star and black

hole LMXBs. Not only does this disc model predict a dense spectrum of power spectral peaks, in contrast to the small number of peaks observed, the frequencies are necessarily the frequencies of nearly circular geodesics. In order for ‘‘hydrodynamic corrections’’ (i.e., gas pressure forces) to be large enough to shift the frequencies by $\sim 15\%$ to bring them into agreement with the data, the disc height would have to be $\sim 0.2 r$, invalidating the narrow ring approximation on which the model is based. The behaviour of the disc frequencies would then differ qualitatively from the behaviour predicted by the narrow ring model.

Next, we investigated geodesics with finite but moderate eccentricities. Once geodesics with finite eccentricities are considered, the geodesic precession hypothesis does not by itself predict a relation between ν_{AP} and ν_{K} (see the discussion in Section 1). In order to create a relation between ν_{AP} and ν_{K} , SV proposed that some physical mechanism keeps r_{p} constant in a given source while r_{a} varies. They suggested that r_{p} may remain constant because it is equal to the radius r_{isco} of the innermost stable circular orbit, the radius r_m at which the magnetic field of the star first couples to the accreting gas, or the equatorial radius R_e of the neutron star. However, there is no physical reason why the periastron radius of an eccentric geodesic cannot be significantly smaller than r_{isco} (see Marković 2000). The magnetic coupling radius decreases as the mass accretion rate increases (Lamb 1989; Ghosh & Lamb 1992; Miller et al. 1998; Psaltis et al. 1999a). Moreover, if the stellar magnetic field is strong enough to truncate orbits at r_m , the motion of the accreting gas will not be purely geodesic motion for a substantial distance outside r_m . The equatorial radius R_e provides a lower bound on r_{p} , but otherwise provides no constraint.

In exploring sequences of geodesics with finite eccentricities, we simply followed SV, who assumed that r_{p} is constant in a given source but that it can be chosen freely for each source to give the best possible fit of the $\nu_{\text{AP}}\text{-}\nu_{\text{K}}$ and $2\nu_{\text{NP}}\text{-}\nu_{\text{K}}$ relations to the observed $\nu_1\text{-}\nu_2$ and $\nu_{\text{L}}\text{-}\nu_{\text{K}}$ correlations. We also assumed that for each source r_{a} can be varied freely to give the best possible agreement between the allowed frequency relation and the observed frequency correlation, requiring only that it exceed r_{p} . Therefore the parameters in this model are the EOS, mass, and spin frequency of the neutron star, the periastron radius r_{p} , and an apastron radius for each pair of kilohertz QPO frequencies that was fit.

We found that the $\nu_{\text{AP}}\text{-}\nu_{\text{K}}$ relations given by the best-fitting sequences of moderately eccentric geodesics, defined as geodesics with $r_{\text{a}}/r_{\text{p}} \lesssim 1.5$, also disagree qualitatively with the kilohertz QPO frequency data. As we explained in detail in Section 3.1 and the Appendix, SV came to a different conclusion in their paper proposing the geodesic precession model because they computed the azimuthal frequency ν_{K} incorrectly. When computed correctly, the azimuthal frequencies of the geodesics cited by SV as giving agreement with the Sco X-1 frequency data miss most of the data points by ~ 100 Hz. *Our investigation shows that the best-fitting sequences of moderately eccentric geodesics disagree qualitatively not only with the kilohertz QPO frequency data on Sco X-1 but also with the data on other sources, regardless of the neutron star model and spin rate assumed.* The reason sequences of such geodesics are unable to fit the data is that although the frequency difference $\Delta\nu \equiv \nu_2 - \nu_1$

decreases with increasing ν_2 , the radial epicyclic frequency $\nu_r = \nu_K - \nu_{AP}$ given by such geodesics decreases much more rapidly with increasing ν_K for any realistic neutron star and any allowed spin rate.

6.1.2 Highly eccentric geodesics

In Section 3.2 we explored whether dropping the requirement that geodesics be only moderately eccentric would allow acceptable fits to the kilohertz QPO frequency data. We were able to find sequences of highly eccentric geodesics that give ν_{AP} - ν_K relations qualitatively similar to the frequency data on some sources, but only by using geodesics with very high eccentricities ($r_a/r_p \gtrsim 3$). We were able to find geodesic sequences that agree qualitatively with the frequencies observed in Sco X-1 and 4U 1728-34, provided that the EOS of neutron star matter is similar to the UU or A18+UIX+ δv_b equations of state, although the fits are not formally acceptable. In general, frequency relations similar to the observed frequency correlations are possible only if values of r_p smaller than r_{isco} are allowed. We were able to find sequences of highly eccentric geodesics that give formally acceptable fits to the GX 17+2 and GX 340+0 kilohertz QPO frequencies; however, only a few frequency measurements have been reported for these sources and the uncertainties are large. The best-fitting geodesic sequence appears to be inconsistent with the GX 5-1 frequency data. In Section 3.3 we showed that geodesic frequencies other than ν_{AP} and ν_K are inconsistent with the frequencies of the kilohertz QPOs.

In order to test the suggestion of SV and SVM that the low-frequency QPOs in the atoll sources and the HBOs in the Z sources are the first overtones of nodal precession frequencies, in Section 3.4 we investigated whether the nodal precession frequencies of the sequences of best-fitting highly eccentric geodesics found in Section 3.2 are consistent with the frequency behaviour of the low-frequency QPOs. We found that the predicted ν_{NP} - ν_K and $2\nu_{NP}$ - ν_K relations are qualitatively different from the ν_L - ν_K and ν_{HBO} - ν_K correlations observed in 4U 1728-34, GX 5-1, and Sco X-1. The predicted $2\nu_{NP}$ - ν_K relation is somewhat similar to the frequency correlation observed in GX 17+2, if the spin rate of this neutron star is 660 Hz. However, the value of χ^2/dof is large (4.3) and the required stellar mass is equal to the maximum stable mass for this spin rate.

Finally, in Section 3.5 we considered the unusual source Cir X-1, which is thought to be a neutron star (see van der Klis 2000). The frequencies ν_L and ν_H of its low-frequency QPO and high frequency ‘hump’ both vary by more than an order of magnitude (their reported ranges are 1-12 Hz and 20-200 Hz, respectively; see Tennant, Fabian & Shafer 1986; Tennant 1987; Shirey 1998; Shirey et al. 1996, 1998, 2000). This makes Cir X-1 a crucial testing ground for any model that seeks to explain the neutron star and black hole QPOs within a single framework. Indeed, without the Cir X-1 data, the evidence for a connection between the black hole and neutron star QPOs would be much weaker (see Fig. 2 of Psaltis et al. 1999b).

We first investigated whether a sequence of moderately eccentric geodesics can be constructed that gives a $2\nu_{NP}$ - ν_{AP} relation similar to the ν_L - ν_H correlation observed in Cir X-1 (ν_{NP} is much too low to be consistent with ν_L). We find that sequences of moderately eccentric geodesics around rapidly

spinning ($\nu_s \gtrsim 650$ Hz) neutron stars can give $2\nu_{NP}$ - ν_{AP} relations that are roughly consistent with the observed ν_L - ν_H correlation for $\nu_H < 100$ Hz. However, only moderately eccentric geodesics around very low mass ($M \lesssim 1.3 M_\odot$ for EOS UU) neutron stars spinning near breakup give relations roughly consistent with both the lower-frequency data and the $\nu_L \approx 12$ Hz, $\nu_H \approx 200$ Hz measurement by Tennant (1987). No quantitative comparison is possible, because no errors have been reported for most of the frequency measurements. We then explored whether using sequences of highly eccentric geodesics would make it easier to construct a frequency relation similar to that observed in Cir X-1. We found that the situation for highly eccentric geodesics is similar to that for moderately eccentric geodesics. The lower-frequency data favour moderately eccentric geodesics that are extremely eccentric ($r_a/r_p \gtrsim 6$) and far from the neutron star ($r_a/R_e \gtrsim 10$). Inclusion of the higher-frequency measurement of Tennant (1987) again makes it much more difficult to find a sequence of geodesics that gives a frequency relation similar to the observed correlation. Only highly eccentric geodesics around stars with very low masses and very high spin rates give frequency relations that pass near all the measurements.

In the majority of cases, the values of r_p required to produce ν_{AP} - ν_K relations similar to the observed kilohertz QPO frequency correlations are substantially larger than the equatorial radius R_e of the corresponding neutron star model (for example, in GX 340+0 the required value of r_p is more than $2R_e$). Where a marginally bound geodesic exists, r_p is also significantly larger than r_{mb} for the best-fit HEG sequences. Hence the geodesic precession hypothesis does not provide any obvious explanation of why the periastron radius should have the required value or of why it should remain fixed in a given source. As discussed in Section 3, it seems impossible to overcome this difficulty for any realistic EOS.

The situation for Cir X-1 is even more serious, because geodesics with apastron radii $r_a \sim 5-50 R_e$ are required to fit the frequency data. Clumps so far from the star are unlikely to produce significant X-ray modulation.

6.2 Expected frequencies and power spectra

Up to this point in our analysis we simply assumed that the dominant modulation frequencies produced by clumps moving on geodesics around a neutron star would be ν_K , ν_{AP} , and $2\nu_{NP}$, as proposed by SV, SVM, and Karas (1999). In Section 4 we carried out extensive numerical simulations to determine the waveforms and power spectra that would actually be produced by geodesic motion of clumps. We considered six effects: occultation of the whole stellar surface, occultation of a bright equatorial band, reflection of radiation by clumps, two models of emission of radiation by clumps, and interaction of clumps with a rarified gaseous disc in the rotation equator of the star. Any orbiting clump model will generally produce a power spectrum that is a superposition of the power spectra produced by these effects.

We find that, contrary to what was simply assumed previously, ν_K , ν_{AP} , and $2\nu_{NP}$ are not the most prominent frequencies generated by orbiting clumps. Instead, most of the power generated by such clumps is typically in peaks of roughly equal power at the radial epicyclic frequency ν_r , at $\nu_K + \nu_r$, and at $\nu_K + 2\nu_r$ (see Table 4). As explained in Sec-

tion 4, the reason for this is that for the general relativistic geodesics that are relevant, the only strictly periodic motion is the radial epicyclic motion. In particular, the azimuthal motion is not periodic. There is usually power at ν_K , but it is always $\lesssim 25\%$ of the power in each of the dominant peaks and there are often many other peaks as strong or stronger. For relevant geodesics, the power at ν_{AP} and at ν_{NP} produced by most mechanisms is $\lesssim 10\%$ of the power in the dominant peaks. We were unable to find any effect or geometry that produces a significant peak at $2\nu_{NP}$. Thus, the frequencies of the significant peaks in the power spectra that would be generated by orbiting clumps are qualitatively different from the frequencies of the peaks observed in power spectra of the kilohertz QPO sources.

Periodic modulation of the X-ray emission by orbiting clumps is possible only if the inclination i of the system, which is expected to be the same as the inclination of the star's spin axis and the normal to the accretion disc, is sufficiently large. More generally, the frequency structure and the relative strengths of the oscillations at different frequencies produced by this mechanism depend sensitively on the inclination of the system. However, there is no evidence for any inclination-dependence of the frequency pattern in the low- or high-frequency QPOs, or even in their relative amplitudes. This is difficult to understand in orbiting clump models.

6.3 Dynamical considerations

In Section 5 we investigated the dynamical constraints on orbiting clump models and the X-ray modulation generated by such models. We find that in order for clumps to persist in geodesic motion for ~ 100 orbits, as required by the coherence of the kilohertz QPOs, their radii must be $\ll 10^{-3}$ of the periastron radius. In order to avoid rapid inspiral caused by drag forces, the density of the gas in the clumps must be $\gg 10^5$ times the density of the interclump medium. In order for clumps to avoid colliding with each other too frequently, the density of the gas in the clumps must be $\gg 10^6$ times the mean density near the star. These densities are extreme.

As discussed in Section 5, the small size required for clumps to persist as long as required by the observed coherence of the kilohertz QPOs means that the fractional modulation of the X-ray flux that can be produced by clumps is $\ll 10^{-6}$. This upper bound is many orders of magnitude smaller than the observed fractional amplitudes, which are $\sim 10^{-2}\text{--}10^{-1}$ (van der Klis 2000).

The very low interclump gas density and the small covering factor by clumps that is required by the geodesic precession hypothesis means that radiation can escape from the clumps and from the stellar surface without suffering significant scattering or absorption. Hence scattering or absorption can have little effect on the frequency content of the waveforms produced by the clumps. Therefore all the peaks at all the frequencies we have discussed should be observable. However, most have not been detected (see, e.g., Jonker et al. 1998).

A related point is that even weakly nonuniform emission from the stellar surface should produce readily observable periodic X-ray oscillations at the stellar spin rate. Again, such oscillations have not been detected (see van der Klis 2000).

A major deficiency of the geodesic precession model is that no attempt has been made to explain what causes the gas in the accretion disc, which is moving along nearly circular streamlines, to break up into clumps moving on highly eccentric geodesics. This would require the sudden removal of a substantial fraction of the angular momentum of the gas in the clumps. Nor has there been any attempt to explain why and how clumps are formed only on geodesics with nearly the same values of r_a and r_p , why these special geodesics have similar frequencies and obey similar frequency relations in sources with very different properties (e.g., accretion rates that differ by factors ~ 30), or why the properties of the special geodesics change with the accretion rate in just the way needed to explain the observed changes in the frequencies of the QPOs. Finally, no explanation has been given of how the clumps dissipate and how the accreting gas reaches the stellar surface (injection of clumps onto geodesics that do not intersect the stellar surface does not by itself produce any accretion onto the star).

6.4 Conclusions

We conclude that there are significant difficulties in interpreting the kilohertz and low-frequency QPOs in the atoll and Z sources as consequences of gas clumps moving along geodesics.

The best-fitting geodesic sequences that can be constructed using moderately eccentric geodesics give frequency relations that differ qualitatively from the kilohertz QPO frequency data. Frequency relations qualitatively similar to the kilohertz QPO data on some sources can be constructed, but only if highly eccentric geodesics are used. Such geodesics are very difficult to accommodate in any physically consistent gas dynamical picture of the accretion flow near the star. The best-fitting $2\nu_{NP} - \nu_K$ and $\nu_{AP} - \nu_K$ relations disagree qualitatively with the low-frequency and kilohertz QPO frequency data, for any realistic neutron star models and allowed spin frequencies. Other geodesic frequencies are qualitatively inconsistent with the observed frequencies.

Modulation by orbiting clumps would not produce strong peaks in the power spectra at the frequencies ν_{AP} , ν_K , and $2\nu_{NP}$ as required by the geodesic precession hypothesis. Instead, the strongest peaks would be at the radial epicyclic frequency ν_r and at $\nu_K + \nu_r$ and $\nu_K + 2\nu_r$, frequencies that are inconsistent with the frequencies observed.

Finally, the dynamical constraints on orbiting clump models make it very difficult to see how clumps of the required density could be formed on highly eccentric geodesics, or how X-ray modulation with the amplitudes observed could be generated by orbiting clumps.

Acknowledgements

The authors thank Mariano Méndez for providing observational data and for many stimulating discussions. The authors are grateful to Dimitrios Psaltis and Luca Zampieri for extensive, detailed discussions of the precession hypothesis and fits to the data, and to Mariano Méndez and Cole Miller for comments on the paper. The authors also thank Scott Hughes, Michiel van der Klis, Tom Loredo, Cole Miller, Sharon Morsink, Luigi Stella, Jean Swank, and William

Zhang for helpful conversations. The authors gratefully acknowledge the hospitality of the Aspen Institute for Physics, where many of these discussions took place. This work was supported in part by NSF grant AST 96-18524 and by NASA grants NAG 5-2925 and NAG 5-8424.

REFERENCES

Akmal, A., Pandharipande, V. R. & Ravenhall, D. G. 1998, *Phys. Rev. C*, 58, 1804

Alpar, A., & Shaham, J. 1985, *Nature*, 316, 239

Armitage, P.J., Natarajan, P. 1999, *ApJ*, 525, 909

Arnett, W.D., Bowers, R.L. 1977, *ApJ Suppl.*, 33, 415

Bethe H.A., Johnson, M.B. 1974, *Nucl. Phys. A*, 230, 1

Bildsten, L. 1998, in *The Many Faces of Neutron Stars*, NATO ASI, Lipari (Dordrecht: Kluwer), C515, 419

Chandrasekhar, S. 1983 *The Mathematical theory of Black Holes*. Oxford University Press, Oxford

Cook, G.B., Shapiro, S.L., Teukolsky, S.A. 1992, *ApJ*, 398, 203

Cook, G.B., Shapiro, S.L., Teukolsky, S.A. 1994a, *ApJ*, 422, 227

Cook, G.B., Shapiro, S.L., Teukolsky, S.A. 1994a, *ApJ*, 424, 823

Di Salvo, T., Méndez, M., van der Klis, M., Ford, E., Robba, N.R. 2000, preprint

Jonker, P.J., et al. 1998, *ApJ*, 499, L191

Kaaret., P., et al. 1999, *ApJ*, 523, 197

Kalogera, V., Psaltis, D. 1999, *Phys. Rev. D*, 61, 024009

Karas, V. 1999, *ApJ*, 526, 953 (K)

Komatsu, H., Eriguchi, Y., Hachisu, I. 1989, *MNRAS*, 237, 355

Komatsu, H., Eriguchi, Y., Hachisu, I. 1989, *MNRAS* 239, 153

Lamb, F.K., Miller, M.C. 2000, in preparation

Lamb, F.K., Shibasaki, N., Alpar, A., & Shaham, J. 1985, *Nature*, 317, 681

Landau, L.D., Lifshitz, E.M. 1976 *Mechanics*. Butterworth-Heinemann

Markwardt, C.B., Strohmayer, T.E., Swank, J.H. 1998, *ApJ*, 512, L125

Marković, D. Companion paper.

Marković, D., Lamb, F.K. 1998, *ApJ*, 507, 316

Méndez, M., et al. 1998, *ApJ*, 505, L23

Méndez, M., van der Klis, M. 1999, *ApJ*, 517, L51

Miller, M.C. 1999a, *ApJ*, 515, L77

Miller, M.C. 1999b, *ApJ*, 520, 256

Miller, M.C., Lamb, F.K. 1993, *ApJ*, 413, L43.

Miller, M.C., Lamb, F.K. 1996, *ApJ*, 470, 1033.

Miller, M.C., Lamb, F.K., Psaltis, D. 1998, *ApJ*, 508, 791

Morsink, S., Stella, L. 1999, *ApJ*, 513, 827

Nozawa, T., Stergioulas, N., Gourgoulhon, E., Eriguchi, Y. 1989, *A&A*, 132, 431

Pandharipande, V. R., Akmal, A., Ravenhall, D. G. 1998, in *Nuclear Astrophysics*, Proc. International Workshop XXVI on Gross Properties of Nuclei and Nuclear Excitations, ed. M. Buballa, N. Noorenberg J. Wambach, & A. Wirzba (Darmstadt: GSI), 11

Pandharipande, V.R., Smith, R.A. 1975, *Phys. Lett.*, 59B, 15

Psaltis, D., Belloni, T., van der Klis, M. 1999b, *ApJ*, 520, L262; [astro-ph/9902130](#)

Psaltis, D., et al. 1998, *ApJ*, 501, L95

Psaltis, D., Norman, C. 2000, [astro-ph/0001391](#)

Psaltis, D., et al. 1999a, *ApJ*, 520, 763

Schaab, C., Weigel, M.K. 1999, *MNRAS* 308, 718

Shirey, R.E. 1998, Ph.D. Thesis, MIT

Shirey, R.E., Bradt, H.V., Levine, A.M., Morgan, E.H. 1996, *ApJ*, 469, L21

Shirey, R.E., Bradt, H.V., Levine, A.M., Morgan, E.H. 1998, *ApJ*, 506, 374

Stella, L., Vietri, M. 1998, *ApJ*, 492, L59

Stella, L., Vietri, M. 1999, *Phys. Rev. Lett.*, 82, 17 (SV)

Stella, L., Vietri, M., Morsink, S. 1999, *ApJ*, 524, L63 (SVM)

Stergioulas, N., Friedman, J.L. 1995, *ApJ*, 444, 306

Strohmayer, T.E. 1999, *ApJ*, 523, L51

Strohmayer, T.E., Zhang, W., Swank, J.H., Smale, A., Titarchuk, L., Day, C. 1996, *ApJ*, 469, L9

Strohmayer, T.E., Zhang, W., Swank, J.H., Lapidus, I. 1998, *ApJ*, 503, L147

Tennant, A.F. 1987, *MNRAS*, 226, 971

Tennant, A.F., Fabian, A.C. Shafer, R.A. 1986, *MNRAS*, 219, 871

van der Klis, M. 1995, in *X-Ray Binaries*, ed. W.H.G. Lewin, J. van Paradijs & E.P.J. van den Heuvel (Cambridge Univ. Press), 252

van der Klis, M. 1998 in the Proceedings of the Third William Fairbank Meeting, Rome June 29–July 4 1998, [astro-ph/9812395](#)

van der Klis, M. 2000, *Ann. Rev. Astr. & Astrophys.*, [astro-ph/0001167](#)

van der Klis, M., Wijnands, R.A.D., Horne, K., Chen W. 1997, *ApJ*, 481, L97

Wijnands, R., van der Klis 1997, *ApJ*, 482, L65

Wijnands, R. et al. 1997a, *ApJ*, 479, L141

Wijnands, R. et al. 1997b, *ApJ*, 490, L157

Wijnands, R. et al. 1998, *ApJ*, 504, L35

Wiringa, R.B., Fiks, V., Fabrocini, A. 1988, *Phys. Rev. C*, 38, 1010

Zhang, W. et al. 1996, *ApJ*, 469, L17

Zhang, W., Strohmayer, T.E., Swank, J.H., ApJ, 500, L167

APPENDIX A: KEPLERIAN (AZIMUTHAL) FREQUENCIES OF ECCENTRIC GEODESICS

In order to clarify the difference between the definition of the Keplerian (azimuthal) frequency of eccentric geodesics and the quantity used by Stella & Vietri (2000; hereafter SV), we first discuss the definition of the Keplerian frequency, then derive expressions for the radial epicyclic and Keplerian frequencies of eccentric geodesics in the Schwarzschild spacetime, and finally explain how we were able to reproduce the curve shown by SV in their Fig. 2. The expressions needed are given by Markovic (2000). However, in order to facilitate comparison with the expressions given by SV, in this appendix we use the notation of SV, whose derivation follows closely the discussion in Chandrasekhar (1983, pp. 100–105).

A1 Definition of the Keplerian frequency

For a test particle moving on an eccentric geodesic, the rate of azimuthal phase advance varies with its radius, and hence only the *average* rate of azimuthal phase advance is meaningful. This is the quantity conventionally denoted $2\pi\nu_\phi$ or $2\pi\nu_K$. In the Schwarzschild spacetime, eccentric geodesics are not closed (because of apsidal precession), the azimuthal motion of a particle moving on such a geodesic is not periodic, and the average rate of azimuthal phase advance is not proportional to the inverse of the time required for the particle to traverse a 2π interval in azimuthal phase (see, e.g., Section 14 of Landau & Lifshitz 1976). However, the radial motion is periodic, with period $1/\nu_r$, where ν_r is the radial epicyclic frequency. The rate at which a particle's azimuthal phase advances depends only on its radius and hence is also

periodic with period $1/\nu_r$. The average rate at which a particle's azimuthal phase advances can therefore be computed by calculating the phase advance during any time interval that is a multiple of half the radial epicyclic period and then dividing by the time interval. For example, if $\Delta\phi$ is the azimuthal phase advance during each radial epicyclic period, then $\nu_\phi = (\Delta\phi/2\pi) \nu_r$.

Instead of using the usual definition of ν_ϕ , SV appear to have assumed that ν_ϕ is the inverse of the time required for the azimuthal phase to advance by 2π . However, as just explained, the rate of azimuthal phase advance of a particle moving on an eccentric geodesic in the Schwarzschild space-time depends on the instantaneous radius of the particle and the azimuthal motion is not periodic. Hence the time required for the particle's azimuthal phase to increase by 2π depends on the assumed initial position of the particle and is not even well-defined; it is not the inverse of the Keplerian frequency. As Fig. A1 shows, the time required for the azimuthal phase to advance by 2π depends sensitively on the starting position used in computing it, even when the eccentricity is relatively small. The non-uniqueness of this time is a consequence of the nonperiodic nature of the azimuthal motion. (The nonperiodic nature of the azimuthal motion is also the reason why the peak at ν_ϕ in power spectra of the X-ray flux modulation produced by eccentric geodesic motion is not very prominent.)

A2 Calculation of the Keplerian and radial epicyclic frequencies ν_K and ν_r

For a non-rotating ($j = 0$) spherical star, equations (20)–(22) of Markovic (2000), which describe the geodesic motion of a particle of unit proper mass, simplify considerably. Following Chandrasekhar (1983), we use the radial variable $u \equiv 1/r$, where r is the radius in Schwarzschild coordinates. Then (see Chandrasekhar 1983, Section 19; Shapiro & Teukolsky 1983, Ch. 12)

$$\begin{aligned} \dot{u}^2 &= (2L^2u^3 - L^2u^2 + 2u + E^2 - 1)u^4 \\ \dot{t} &= \frac{E}{1-2u} \\ \dot{\phi} &= Lu^2, \end{aligned} \quad (\text{A1})$$

where E and L are, respectively, the conserved energy and angular momentum of the particle. Here all distances are in units of GM/c^2 and all times, in units of GM/c^3 .

From equations (A1) it follows that

$$\left(\frac{du}{d\phi}\right)^2 = 2(u - u_1)(u - u_2)(u - u_3), \quad (\text{A2})$$

where $u_1 = 1/r_a$, $u_2 = 1/r_p$, and $u_3 > u_2 > u_1$. Introducing $\mu \equiv 1/l$ and evaluating the coefficients of the polynomials in u in equations (A1) and (A2), one finds

$$u_1 = \frac{1-\epsilon}{l}, \quad u_2 = \frac{1+\epsilon}{l}, \quad u_3 = \frac{1}{2} - \frac{2}{l}, \quad (\text{A3})$$

and

$$\begin{aligned} \frac{1}{L^2} &= \frac{1}{l} [1 - \mu(3 + \epsilon^2)] \\ \frac{E^2}{L^2} &= \frac{1}{l} [(1 - 2\mu)^2 - 4\epsilon^2\mu^2], \end{aligned} \quad (\text{A4})$$

where $l \equiv 2/(u_1 + u_2)$ and $\epsilon \equiv (r_a - r_p)/(r_a + r_p) = (u_2 - u_1)/(u_2 + u_1)$ is the eccentricity.

From equations (A1)–(A4), we obtain

$$\begin{aligned} \left(\frac{d\chi}{d\phi}\right)^2 &= 1 - 2\mu(3 + \epsilon \cos \chi) \\ &= (1 - 6\mu + 2\epsilon\mu) [1 - \kappa^2 \cos^2(\chi/2)], \end{aligned} \quad (\text{A5})$$

where $\kappa^2 \equiv 4\epsilon\mu/(1 - 6\mu + 2\epsilon\mu)$ and χ is defined implicitly by

$$u \equiv \frac{1 + \epsilon \cos \chi}{l}. \quad (\text{A6})$$

Equations (A1) and (A5) yield

$$\begin{aligned} \frac{dt}{d\chi} &= \frac{dt}{d\phi} \frac{d\phi}{d\chi} \\ &= \left(\frac{E}{1-2u}\right) \left(\frac{1}{Lu^2}\right) \frac{1}{[1-2\mu(3+\epsilon\cos\chi)]^{1/2}} \\ &= \frac{l^{3/2} [(1-2\mu)^2 - 4\epsilon^2\mu^2]^{1/2} (1+\epsilon\cos\chi)^{-2}}{[1-2\mu(1+\epsilon\cos\chi)][1-2\mu(3+\epsilon\cos\chi)]^{1/2}}. \end{aligned} \quad (\text{A7})$$

As χ increases from 0 to 2π , the particle executes one full period of its *radial* motion, moving from its periastron radius $r_p = 1/u_2$ to the apastron radius $r_a = 1/u_1$ and back to r_p again. Hence the radial epicyclic frequency ν_r is given by

$$\frac{1}{\nu_r} = \int_0^{2\pi} \left(\frac{dt}{d\chi}\right) d\chi. \quad (\text{A8})$$

One can relate ν_r to the Newtonian frequency $\nu_N = a^{-3/2}/2\pi$ using the expression $a = (1/u_1 + 1/u_2)/2 = l/(1 - \epsilon^2)$ for the semi-major axis a of the geodesic. The result is

$$\nu_r = 2\pi\nu_N \frac{1}{(1-\epsilon^2)^{3/2}} \frac{1}{[(1-2\mu)^2 - 4\epsilon^2\mu^2]^{1/2}} \frac{1}{f(\epsilon, \mu)}, \quad (\text{A9})$$

where

$$f(\epsilon, \mu) \equiv \int_0^{2\pi} \frac{(1 + \epsilon \cos \chi)^{-2} d\chi}{[1 - 2\mu(1 + \epsilon \cos \chi)][1 - 2\mu(3 + \epsilon \cos \chi)]^{1/2}}. \quad (\text{A10})$$

As the particle executes one period of its radial epicyclic motion, its azimuth ϕ increases by (see eq. A5)

$$\Delta\phi = \frac{1}{\sqrt{1-6\mu+2\epsilon\mu}} \int_0^{2\pi} \frac{d\chi}{[1-\kappa^2\cos^2(\chi/2)]^{1/2}}. \quad (\text{A11})$$

The mean rate of advance of the particle's azimuth ϕ is $2\pi\nu_\phi = \nu_r\Delta\phi$. Hence

$$\nu_\phi = \nu_r \frac{\Delta\phi}{2\pi}. \quad (\text{A12})$$

Quite generally, $\Delta\phi > 2\pi$, so the geodesics are not closed.

A3 Calculation of SV

Equations (A9) and (A10) for the radial epicyclic frequency ν_r are the same as equations (2) and (3) given by SV. However, instead of computing the azimuthal frequency ν_ϕ given by equations (A11) and (A12), SV appear to have computed

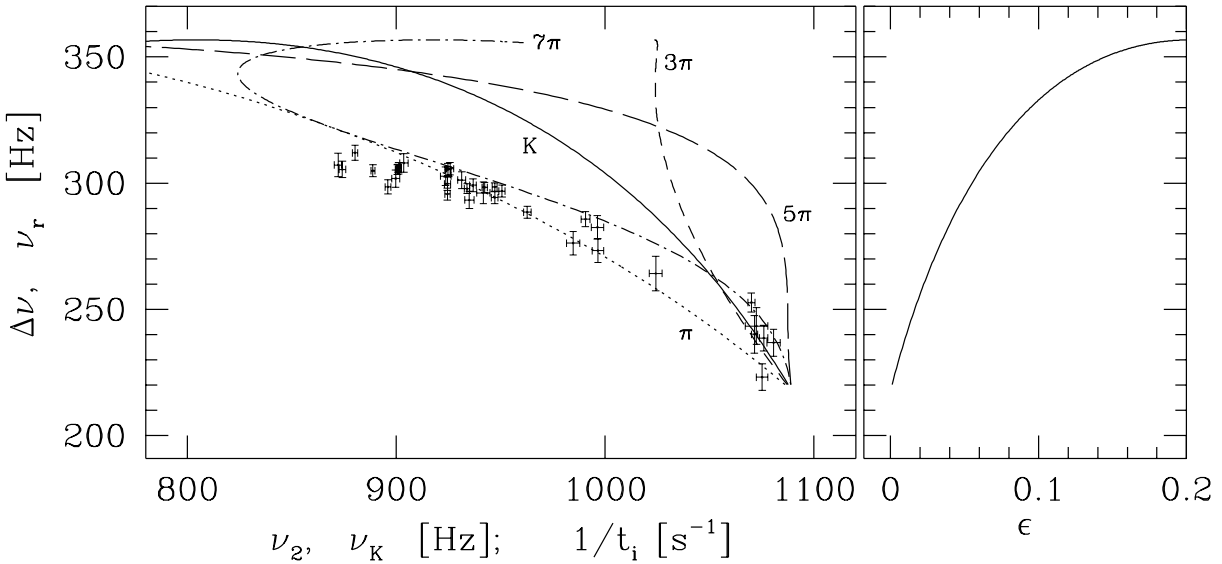


Figure A1. The data points in the left panel show the $\Delta\nu$ - ν_2 correlation observed in Sco X-1. The solid curve labeled K in the left panel shows how the radial epicyclic frequency ν_r varies with the Keplerian (azimuthal) frequency ν_K for the sequence of geodesics specified in the caption of Fig. 2 of Stella & Vietri (1999). For these geodesics, the eccentricity ϵ increases with increasing ν_r , as shown in the right panel. The dotted curve labeled π in the left panel shows ν_r as a function of $1/t_\pi$, the inverse of the time required for a particle to advance in azimuthal phase from π radians before apastron to π radians after apastron. The short dashed curve shows ν_r as a function of $1/t_{3\pi}$, the inverse of the time required to advance from π radians after apastron to 3π radians after apastron. The long dashed curve shows ν_r as a function of $1/t_{5\pi}$, the inverse of the time required to advance from 3π radians after apastron to 5π radians after apastron. The dash-dotted curve shows ν_r as a function of $1/t_{7\pi}$, the inverse of the time required to advance from 5π radians after apastron to 7π radians after apastron.

the time required for a particle to advance through an azimuthal interval of 2π centered about the azimuthal phase of its apastron and then to have identified the inverse of this time with ν_ϕ , which it is not.

If a particle has $\chi = \chi_0$ initially, its azimuthal phase will have increased by 2π at $\chi = \chi_1$, where χ_1 is given implicitly by

$$2\pi = \frac{1}{\sqrt{1-6\mu+2\epsilon\mu}} \int_{\chi_0}^{\chi_1} \frac{d\chi}{[1-\kappa^2 \cos^2(\chi/2)]^{1/2}}. \quad (\text{A13})$$

In the Schwarzschild spacetime, the radial motion of a particle is always slower than its azimuthal motion and hence $\chi_1 - \chi_0 < 2\pi$. As noted above, the rate at which the particle's azimuthal phase advances depends on its radius and its motion in the azimuthal direction is nonperiodic. Hence, the time required for the azimuthal phase of a particle to advance by 2π depends on its initial position, i.e., on χ_0 .

According to SV, the azimuthal frequency is given by the inverse of their equation (2) (our eq. [A9]), but with $f(\epsilon, \mu)$ given by their equation (3) (our eq. [A10]), the integral in their equation (3) taken over 0 to χ_c rather than 0 to 2π , and χ_c given implicitly by their eq. (4). This ‘azimuthal frequency’ is the inverse of the time required for the particle to traverse the azimuthal phase interval of 2π centered on the particle's apastron, if the integration in SV's eq. (3) is meant to be over $\pi - 2\chi_c$ to $\pi + 2\chi_c$, rather than 0 to χ_c , and their expression for k is instead an expression for k^2 .[†]

[†] SV follow Chandrasekhar's (1983) notation, but use x instead of χ . Hence they use the variable $\gamma \equiv \pi/2 - \chi/2$ rather than χ .

Indeed, we were able to reproduce the ν_r vs. ‘azimuthal frequency’ curve shown in Fig. 2 of SV (see below) by using as the ‘azimuthal frequency’ the inverse of the time required for χ to increase from χ_0^* to χ_1^* , where $\chi_1^* - \pi = \pi - \chi_0^*$. (χ_0^* is related to χ_c by $\chi_0^* = \pi - 2\chi_c$.) This is the inverse of the time required for the particle to traverse the 2π phase interval centered on its apastron phase (see eq. [A6]). Fig. A1 shows that the times required for the azimuthal phase of the particle to advance by successive additional intervals of 2π are all different from one another.

The rate of azimuthal phase advance is smallest at apastron, and hence the azimuthal phase interval used by SV gives the smallest possible inverse time and thus the flattest possible ν_r -inverse time curve. This flattest possible curve is shown as the dotted curve in Fig. A1, for the parameters Stella & Vietri list in the caption of their Fig. 2. Fig. A1 shows that any other choice of inverse time would have given a ν_r -inverse time curve much further from the Sco X-1 data. These inverse times are not relevant in any case, because none of them are equal to the azimuthal frequency of the particle. As shown in Section 3.1, the best-fitting ν_r - ν_ϕ relation is qualitatively different from the correlation between the kilohertz QPO frequencies observed in Sco X-1.

in their eq. (4), which corresponds to our eq. (A13). Also, they write their eq. (4) in terms of the integral over only the first half of the 2π phase interval centered at the particle's apastron.